Parsing the Oceanic Calcium Carbonate Cycle:

A Net Atmospheric Carbon Dioxide Source, or a Sink?

Stephen V. Smith

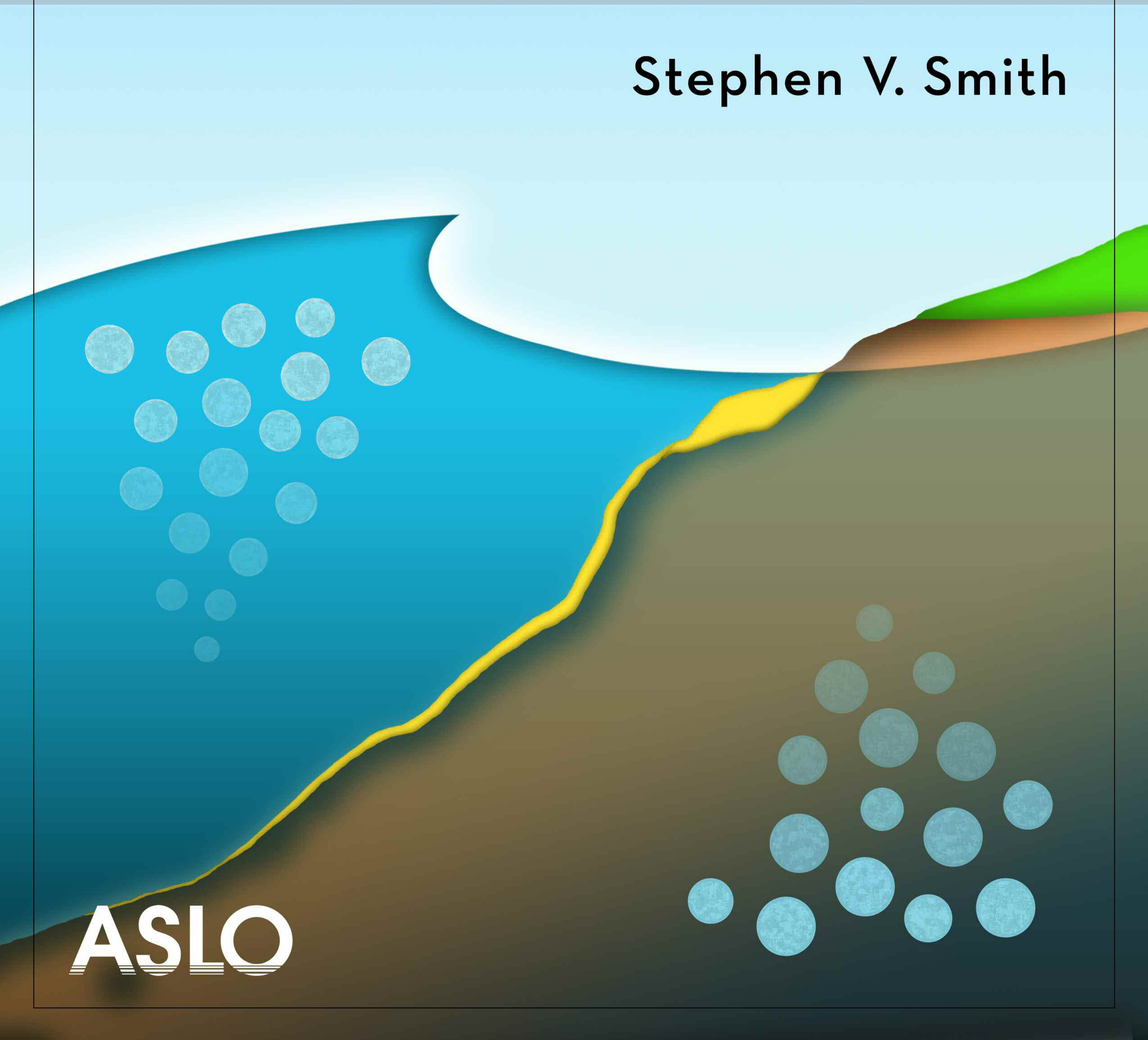

ASLO

Parsing the oceanic calcium carbonate cycle: a net atmospheric carbon dioxide source, or a sink?

Stephen V. Smith
Emeritus Professor of Oceanography, University of Hawaii
49 Las Flores Drive, Chula Vista, CA 91910

2013

ISBN: 978-0-9845591-2-1

DOI: 10.4319/svsmith.2013.978-0-9845591-2-1

Limnology and Oceanography e-Books
www.aslo.org/books/

Correct citation for this e-Book: Smith, S.V. 2013. Parsing the oceanic calcium carbonate cycle: a net atmospheric carbon dioxide source, or a sink? L&O e-Books. Association for the Sciences of Limnology and Oceanography (ASLO) Waco, TX. 10.4319/svsmith.2013.978-0-9845591-2-1

Cover illustration by Jason Emmett

Preface

Environmental scientists have watched the progression of the "Keeling Curve" recording the rise of atmospheric CO_2 at Mauna Loa, Hawaii, for the past 50-plus years, from 315 parts per million by volume (ppmv) in 1958 to its present (2012) level of about 393 ppmv (Keeling 1960; Scripps and subsequent NOAA data available at http://www.esrl.noaa.gov/gmd/ccgg/trends/; last accessed 3 Mar 2012). The 2012 value is about 25% above the value at the beginning of the Mauna Loa record and 40% above the value in about 1740 (Lüthi et al. 2008). Atmospheric CO_2 has apparently not been this high since at least 20 million years ago (Pagani et al. 2005). This rapid, recent CO_2 rise is widely attributed to human activities: primarily, the burning of fossil fuels; secondarily, changing patterns of land cover and land use (Canadell et al. 2007).

Crutzen (2002) suggested that the Holocene geological epoch has now been supplanted by the Anthropocene epoch—the human-dominated epoch. He observed that the inception of the modern rise in carbon dioxide (and methane) concentrations in the atmosphere "…happens to coincide with James Watt's design of the steam engine in 1784."

As a result of the above and related observations and obvious environmental responses to the rising CO_2, the global carbon cycle has come under increasing attention in terms of human effects on our planet. The most immediate physical-chemical effects are changing global climate patterns and increasing acidity of surface ocean waters. Rising temperature, altered weather patterns, and other aspects of climate change occur as elevated CO_2 in the atmosphere alters the heat balance of the planet by absorbing increasing amounts of infrared radiation. The global hydrological cycle is, in turn, being altered. Ocean acidification occurs as CO_2 is absorbed into surface seawater and increases the carbonic acid content of the ocean. Changing climate, hydrologic patterns, and seawater composition are altering (to greater or lesser extent) all biotic habitats on the planet. For example, coral reefs and other calcifying ecosystems and organisms in the ocean are apparently at risk from increasing ocean acidity (see Gattuso and Hansson 2011).

These CO_2-induced environmental changes caused by human perturbations of the carbon cycle have important socioeconomic ramifications as well (including, but hardly limited to, damage from extreme weather, flooding of the coastal zone from sea level rise, "cheap" extraction of the most readily available fossil fuels, food security issues, as agricultural soil fertility is lost and ocean composition is altered, and the list goes on). Most informed environmental scientists would agree with most of my general assertions, loud disclaimers from skeptics notwithstanding. Details of the global responses to rising CO_2 continue to be discovered and discussed.

The preceding comments set the stage for the analysis presented here. I do not intend to discuss the broad consequences of the altered carbon cycle further in this book. Rather, I explore one set of details in the global carbon cycle: the relationship between the oceanic $CaCO_3$ cycle and CO_2 gas exchange between the ocean and atmosphere.

I have, I believe, unearthed some surprising aspects with respect to $CaCO_3$-mediated CO_2 gas exchange. The air-sea exchange of CO_2 associated with $CaCO_3$ reactions appears to be poorly represented by conventional analyses. This apparently rather esoteric and academic topic is, in my opinion, directly relevant to the pragmatic issue of global changes brought about by anthropogenic activity for the following reason. To gain quantitative understanding of the Anthropocene carbon cycle and to learn to manage that cycle more effectively, we must get the details of the pre-Anthropocene carbon cycle "right."

The devil is in the details.

The analysis presented here can be traced back through field, laboratory, and theoretical studies on oceanic geochemistry, biology, and geology, to publications from two momentous expeditions of discovery in the mid-19th century (voyage of the HMS *Beagle*, 1832-1836, and the *Challenger* Expedition, 1872-1876). Relevant research conducted primarily since the early 1940s is described in some detail in this book, and lays out an evolving understanding of carbonate geochemistry. I have relied heavily on the World Ocean Database 2009 database as a source for the CO_2-related composition of the contemporary world ocean. Results of these analyses are then used to forecast to the "post-modern" ocean of a few decades from now, and to hindcast into the geological record.

The analysis has greatly benefited from discussion with and critical comments by two of my oldest friends and professional colleagues, Bob Buddemeier and Fred Mackenzie. In particular, Bob finally convinced me that the temporal variation of surface-ocean Ψ might be significant: he was right! Discussions with John Milliman have provided insight from his initial assessment and subsequent updates of the global ocean $CaCO_3$ budget. Many years ago, when I first began exploring the relationships between oceanic $CaCO_3$ precipitation and sea-air CO_2 flux, Bob Garrels and Bob Berner provided "healthily skeptical" counterarguments to my analyses; more recently, Rane Curl has taken up the same discussion with me.

Victor Camacho-Ibar, John Ware, Dennis Swaney, Tim Hollibaugh, and Wei-Jun Cai have also provided thoughtful critical comments on the manuscript. I also thank two anonymous reviewers for their constructive comments on the original submission of this manuscript.

I thank Reiner Schlitzer for his development of the Ocean Data View (ODV) software, for his assistance to me as I learned how to use the software, and particularly, for providing me with a pre-release version of the software (version 4.3.11.2), the first version of ODV that included calculations of CO_2-related variables.

Finally, I dedicate this contribution to the memory of Keith Chave, my PhD thesis advisor many years ago and long-time friend and colleague. Among many other things, and paraphrasing the title of a thought-provoking publication of his (Chave 1968), Keith encouraged me to "think unconventionally" about $CaCO_3$ in the ocean.

Stephen V. Smith
Chula Vista, California

Table of Contents

Parsing the oceanic calcium carbonate cycle: a net atmospheric carbon dioxide source, or a sink?

Stephen V. Smith
Emeritus Professor of Oceanography, University of Hawaii, 49 Las Flores Drive, Chula Vista, CA 91910

E-mail: svsmit@gmail.com

Abstract

The "standard" equation used to describe $CaCO_3$ precipitation and dissolution is

$$Ca^{2+} + 2HCO_3^- = CaCO_3 + CO_2 + H_2O.$$

As written, the equation somewhat overestimates the ratio of CO_2 gas flux to $CaCO_3$ precipitation and dissolution considered individually in the contemporary ocean, and it substantially misestimates the flux associated with the net reaction (i.e., precipitation minus dissolution).

The equation can be adjusted to reflect this molar flux ratio more accurately:

$$Ca^{2+} + (1 + \Psi)HCO_3^- + (1 - \Psi)OH^- = CaCO_3 + \Psi CO_2 + H_2O,$$

where Ψ is a coefficient related to the HCO_3^- buffer capacity of seawater and is a function of temperature and pCO_2. When the equation is applied to contemporary hydrographic data for the world ocean, it is found that Ψ presently varies from an average of ~0.63 in low to mid-latitude surface waters (the primary sites of $CaCO_3$ production) to ~0.85 below 500 m throughout the ocean (where most dissolution occurs). In addition to this vertical variation, surface ocean values for Ψ have varied substantially over time, primarily in response to variations in atmospheric pCO_2.

The $CaCO_3$-generated flux of CO_2 between ocean and atmosphere and the direction of flux are strongly affected by the vertical variations in Ψ interacting with amounts and relative proportions of pelagic versus benthic $CaCO_3$ production, export, dissolution, and accumulation.

Most pelagic $CaCO_3$ production is transported downward by particle fallout from production sites high in the water column and dissolves lower in the water column; only a small fraction of pelagic production is incorporated into the sedimentary record. As a consequence of vertically variable Ψ in the sites dominated by $CaCO_3$ production and dissolution, net reactions leading to the accumulation of pelagically derived $CaCO_3$ in the contemporary ocean absorb more CO_2 from the atmosphere than is released during production. By contrast, most benthic $CaCO_3$ production accumulates in the sediments, with little dissolution. Therefore net accumulation of benthically derived $CaCO_3$ is a net source of CO_2 release to the ocean, and ultimately to the atmosphere.

Net $CaCO_3$ reactions in the contemporary ocean are a slight net source of CO_2 release to the atmosphere. As a geochemical consequence of vertically and temporally variable Ψ, as well as the relative contribution of benthic versus planktonic calcifying communities to $CaCO_3$ production and accumulation, the role of gross and net $CaCO_3$ production as a source or a sink of atmospheric CO_2 varies over time. Geochemical consequences of these observations and calculations with respect to air-sea CO_2 flux are explored for the present and post-modern (increasingly acidified) ocean; for changing shallow benthic habitat area and Ψ over the past 120,000 years (the last glacial-interglacial cycle); and over Phanerozoic geological time (~550 million years).

DOI: 10.4319/svsmith.2013.978-0-9845591-2-1

Chapter 1. Introduction

The analysis presented here has two foundation blocks, both literally and figuratively. Coral reefs are iconic examples of the first block: shallow-water calcareous sediment and (eventually) limestone formation. Charles Darwin described the structure and distribution of coral reefs in his 1842 book, which may be second in his scientific contributions only to his writings on evolution. His theory on the origin of coral atolls, the concept that large volumes of shallow-water benthic limestone accumulate on sinking volcanic islands, initially met with skepticism. The theory was proved to be correct for most atolls more than a century later, by drilling of Pacific atolls (Ladd and Schlanger 1960; Ladd et al. 1967). Other shallow, benthic, calcifying communities, such as extensive banks dominated by calcareous green algae, oyster reefs, the diverse biotic communities found in temperate-climate kelp beds, also contribute to calcareous sediment formation (e.g., Milliman 1974)

The second foundation block has been known since the *Challenger* Expedition of the 1870s: calcareous pelagic sediments that are common throughout much of the world ocean area (Murray and Renard 1891), establishing the clear importance of deep ocean carbonate deposits. A further, important aspect of pelagic sediments is that the percentage of $CaCO_3$ in these sediments decreases dramatically in water depths greater than 3000-4000 m (Sverdrup et al. 1942). The famous White Cliffs of Dover, on the south coast of England, are examples of uplifted Cretaceous chalk beds found throughout much of Europe. The Dover beds are composed primarily of the pelagic calcareous algae, coccolithophorids (although there is also a significant benthic component to these relatively shallow water deposits: see review by Kennedy and Garrison 1975).

Besides their prominence as major sedimentary deposits in the contemporary ocean, shallow and deep water limestone deposits are found throughout much of the geological record. The comparative roles of shallow versus deep water carbonate sediment and limestone production, dissolution, and accumulation with respect to air-sea exchange of carbon dioxide gas are the subjects of the analysis presented here. Two mineral forms of calcium carbonate (calcite, including and Mg-rich calcite, and aragonite), both primarily precipitated by biogenic processes, are the major forms of carbon found in contemporary oceanic sediments. Note that magnesium-rich calcite can contain up to about 30% substitution of Mg^{+2} for Ca^{+2} in the calcite mineral structure. Other cations (e.g., Sr^{+2}) can also substitute for Ca^{+2}. Throughout this analysis, "$CaCO_3$" should be taken to include the carbonate minerals, calcite and aragonite, with these minor elemental substitutions for Ca^{+2}. The purpose of the analysis presented here is to explore and clarify aspects of these oceanic $CaCO_3$ fluxes in the global CO_2 cycle.

In particular, what is the air-sea CO_2 flux associated with $CaCO_3$ precipitation and dissolution? And what is the significance of that flux? Re-reading papers about carbon flux on the Bahama Banks and elsewhere written over approximately the past 100 years, and reflections on my own research on the carbon cycle in various calcifying oceanic ecosystems over the past 40-plus years, have focused my attention on some interesting peculiarities in the $CaCO_3$ reactions, on important differences in net $CaCO_3$ reactions between pelagic and benthic calcifying systems in the global ocean, and on the CO_2 fluxes associated with those systems at the present and recent past, into the near future, and over the past interglacial-glacial cycle. Some discussion of $CaCO_3$ reactions and CO_2 flux over geological time is also presented.

Organic carbon reactions [production – respiration] and $CaCO_3$ reactions [precipitation – dissolution] are the dominant biogeochemical processes in the oceanic carbon cycle (e.g., Raven and Falkowski 1999). These may be considered "reaction couplets," with the gross forward and backward reactions greatly exceeding net fluxes.

Of these two reaction couplets, organic metabolism cycles carbon far more rapidly. Organic carbon production in, and export from, the contemporary surface ocean total about 900×10^{12} mol C y^{-1} (Laws et al. 2000; Lee 2001). This so-called "export production" accounts for only about 20% of oceanic net primary production (Laws et al. 2000). Only about 8×10^{12} mol y^{-1} of the export production are buried in the sediments (Hedges and Keil 1995; Burdige 2005); that is, about 99% of export production (99.8% of net primary production) is respired. Hedges and Keil (1995) estimated that about 12×10^{12} mol y^{-1} of the organic C burial in oceanic sediments occurs in deltaic, shelf, and upper slope sediments. Burdige (2005) calculated that about 40% of the organic matter in these continental margin sediments is of terrestrial origin, further evidence that almost all organic C produced in the ocean is respired, rather than buried.

$CaCO_3$ production, also primarily in the upper ocean, totals about 90×10^{12} mol C y^{-1}, only 10% of organic C export production (Milliman and Droxler 1996; Lee 2001). In contrast to organic C oxidation, about one-third of $CaCO_3$ production (~30×10^{12} mol y^{-1}) escapes dissolution and accumulates in oceanic sediments (Milliman and Droxler 1996).

According to these estimates of organic matter and $CaCO_3$ burial, organic C accounts for 22% of total C burial in contemporary marine sediments. This percentage is consistent with estimations summarized by Lerman and Mackenzie (2005) that organic C accounts for 17% to 30% of total sedimentary C. Thus, the $CaCO_3$ production—dissolution couplet—while smaller than organic production – respiration in absolute rates of C cycling, represents a substantially larger net transfer of C from dissolved inorganic material to solid form, and to eventual accumulation.

The net accumulation of particulate (primarily inorganic) C is, in turn, a significant driver of CO_2 flux between the atmosphere and ocean. Understanding the natural biogeochemical flux of CO_2 between the atmosphere and ocean is important to understanding how human activities are modifying the oceanic carbon cycle. Analysis presented here derives a modification to "conventional wisdom" on the CO_2 flux associated with $CaCO_3$ reactions in seawater. The analysis presented here demonstrates that amount of CO_2 flux associated with net $CaCO_3$ accumulation in the ocean and even the direction of that CO_2 flux require substantial revision.

Chapter 2. Historical Background

The following equation is often used to describe the precipitation and dissolution of $CaCO_3$ (e.g., Morse and Mackenzie 1990; Wollast 1994; Raven and Falkowski 1999; Berner 2004a):

$$Ca^{2+} + 2HCO_3^- = CaCO_3 + CO_2 + H_2O. \tag{1}$$

The equation states that one mole of $CaCO_3$ precipitation consumes two moles of dissolved bicarbonate ions. According to this equation as written, one mole of HCO_3^- is incorporated into $CaCO_3$; the other mole is converted to aqueous free CO_2. In the reverse reaction, dissolution moves two moles of C (one from free CO_2; one from $CaCO_3$) back to HCO_3^-. If the water undergoing either the precipitation or the dissolution reaction is in gaseous equilibrium with the atmosphere, then the accumulated CO_2 gas pressure difference from the free CO_2 transfers gas to or from the atmosphere and returns that pressure difference back toward 0. In the absence of atmospheric exchange, the reaction results in variations of free CO_2 (and CO_2 partial pressure) in the water. To summarize, the molar ratio of free CO_2 transfer to $CaCO_3$ reaction (in the direction of either $CaCO_3$ precipitation or dissolution), as predicted by Eq. 1, is 1:1.

Qualitatively, the equation is not in question. The Bahama Banks and other marine ecosystems of the Caribbean Sea have been sites of detailed research on marine $CaCO_3$ precipitation at least since the studies of Drew (1913). Of particular relevance to the present analysis, C. L. Smith (1940a, 1940b) studied the hydrography and changing chemical composition of seawater flowing across the Bahama Banks and demonstrated the following sequence of events as water moves across the Banks: The water impinging upon the Banks is approximately in pCO_2 equilibrium with the atmosphere; $CaCO_3$ precipitates, lowering total alkalinity (TA) and total CO_2 (TCO_2); CO_2 partial pressure (pCO_2) rises above atmospheric values; as a consequence of elevated pCO_2, the water degasses; pCO_2 decreases back toward equilibrium with the atmosphere.

As far as I am aware, Smith's study (1940a, 1940b) in the Bahamas was the first ecosystem-scale attempt at a $CaCO_3$-CO_2 mass-balance analysis in an aquatic environment, although there were earlier papers (cited by Smith [1940a, 1940b]) documenting both the $CaCO_3$ saturation state of surface seawater and $CaCO_3$ precipitation from seawater on the Bahama Banks and elsewhere. Smith's data (1940a, 1940b) were sufficiently precise to demonstrate that both forms of TCO_2 loss described by Eq. 1 (i.e., loss to $CaCO_3$ and loss to CO_2 gas) occur in response to $CaCO_3$ precipitation, but the data were insufficiently precise to demonstrate any quantitative discrepancy between his results and the prediction of that equation.

More precise data were collected on the Bahama Banks by Broecker and Takahashi (1966). Those authors qualitatively confirmed the pattern of $CaCO_3$ precipitation and CO_2 gas flux observed by Smith (1940a, 1940b) and several subsequent authors cited by Broecker and Takahashi (1966). More importantly, Broecker and Takahashi (1966) observed that the ratio of CO_2 gas evasion to $CaCO_3$ precipitation on the Bahama Banks was about 0.6, not 1.0. These results supported Eq. 1 qualitatively, but not quantitatively. Broecker and Takahashi (1966) discussed the discrepancy, inferred that the role of net organic carbon metabolism was minor (based largely on the very low organic C content of the $CaCO_3$ sediments of the Bahama Banks), and concluded that the Bahama CO_2 budget could not be balanced (with respect, implicitly, to Eq. 1).

My colleagues and I subsequently re-examined data from seawater $CaCO_3$ precipitation experiments that had been conducted by Wollast et al. (1980) in Bermuda. From those data, we calculated a molar ratio of gas evasion to $CaCO_3$ flux similar to the observations of Broecker and Takahashi (1966) (i.e., ~0.6) (Smith 1985; Ware et al. 1991). Under the experimental conditions Wollast et al. (1980) imposed, organic carbon reactions can be ruled out as a contributing factor to the TCO_2 fluxes calculated from their data set. Wollast et al. (1980) concluded that $CaCO_3$ precipitation did, indeed, cause gas efflux from the water, as expected from Eq. 1. Those authors apparently did not note, however, the quantitative discrepancy in their experimental data between the expected and observed gas flux:precipitation ratio.

The role of any individual aquatic system with respect to net transfer of CO_2 between the ocean and atmosphere in response to $CaCO_3$ reactions has traditionally been assumed to depend on the sum of forward and reverse reactions according to Eq. 1. Aquatic systems precipitating (and dissolving) $CaCO_3$ also produce and consume organic carbon, according to a reaction that can be represented in a highly simplified form by the following equation:

$$CO_2 + H_2O = CH_2O + O_2. \tag{2}$$

As noted in the introduction, the organic C reaction couplet in the ocean typically turns over carbon far more rapidly than the $CaCO_3$ reaction couplet. Further, organic C production (the forward reaction represented by Eq. 2) requires the availability of light; therefore, the forward reaction shuts down at night and shuts down in the oceanic water column below the photic zone. In contrast, respiration (the back-reaction of Eq. 2) occurs independently of light variation, as long as labile organic carbon and oxygen are available for the oxidation reaction.

The work by Kinsey (1972) apparently represents the first published direct quantitative use of CO_2-related measurements (pH, TA) to measure both organic C metabolism and $CaCO_3$ production on a coral reef. Kinsey also measured dissolved oxygen flux as an independent estimate of organic production. High primary production but low net organic production of coral reef flats was, by this time, well-established for various Pacific coral reefs based on dissolved oxygen changes as water flowed across the reef flats (notably, Sargent and Austin 1954; Odum and Odum 1955; Kohn and Helfrich 1957). Because of the very short water residence times on these reef flats, even rapid absolute rates of $CaCO_3$ and organic C reactions resulted in only small changes in water composition.

I began study of C flux in tropical–subtropical calcifying systems on Enewetak (then usually spelled "Eniwetok") Atoll in 1971, during the *Symbios* Expedition (see Johannes et al. 1972; D'Elia and Harris 2008). My work there was descriptive, on two reef flats with water residence times of a few minutes (Smith 1973). I measured pH and TA, as well as estimating water volume transport rates across the reef flats. On these reef flats, as well as the ocean as a whole, organic C production (only occurring in the light) proceeds far more rapidly than $CaCO_3$ production. Integrated over the light-dark cycle (organic production and respiration), net organic production on coral reef flats is typically low and difficult to distinguish from 0.

Smith and Pesret (1974) turned to the Fanning Atoll (now called "Tabuaeran") lagoonal reef system, with a water exchange time of about a month, in an attempt to use pH and TA measurements as a direct—and unequivocal—measure of net organic production. We used water and salt budgets to estimate water exchange time. Even with this relatively long water exchange time, net organic metabolism was indistinguishable from 0. I subsequently began using nutrient (primarily phosphate, DIP) fluxes as proxies for net organic metabolism in lagoonal reef systems and $CaCO_3$-producing embayments with long water residence times (weeks to months) and large signals of TA and TCO_2 change, to develop a general understanding of C flux in calcifying systems (leading eventually to Smith and Jokiel 1978; Smith and Atkinson 1984; Smith 1984; among other studies). Water exchange rates were estimated in these studies by means of salt budgets as water aged in the systems and rainfall minus evaporation altered the salinity.

An important conclusion of these papers was that these calcifying systems with relatively long residence times typically have very low, positive rates of net organic carbon production even though the communities of these systems typically include coral reefs, benthic algae, and seagrass beds, all of which have high instantaneous rates of organic metabolism. As a result of the low rates of net organic metabolism for these systems, the biogeochemically induced TCO_2 fluxes in such systems are dominated by $CaCO_3$ reactions and resultant sea-to-air CO_2 fluxes.

I eventually began more theoretical consideration of the CO_2 system in calcifying oceanic systems. Smith (1985), Smith and Veeh (1989), and Ware et al. (1991) used the apparent dissociation constants for carbonic acid in seawater to demonstrate that the Broecker and Takahashi (1966) observations about the CO_2 exchange:$CaCO_3$ reaction ratio of about 0.6 on the Bahama Banks has general application for seawater in equilibrium with the atmosphere and at temperatures typical for $CaCO_3$ precipitation (~ 25°C). Ware et al. (1991) referred to this as the "0.6 rule."

High-precision pCO_2, TA, TCO_2, and pH measurements reported by Kawahata et al. (1997) for two coral reef systems in the Western Pacific Ocean (Palau barrier reef, Majuro atoll lagoon) further confirmed that changes in water composition in those systems closely conform to the "0.6 rule" for $CaCO_3$ precipitation, with a very small component of water composition change in response to organic metabolism.

Use of a surface ocean gas evasion:$CaCO_3$ precipitation ratio of 0.6 rather than 1.0 has, by now, been incorporated into several global budgets or models of atmosphere-ocean carbon flux associated with $CaCO_3$ reactions (e.g., Sundquist 1993; Vecsei and Berger 2004; Mackenzie et al. 2005; Lerman and Mackenzie 2005).

Frankignoulle et al. (1994) derived a further, important, generality about the CO_2 flux:$CaCO_3$ precipitation ratio. Those authors pointed out that this ratio is actually not constant. They demonstrated that the ratio increases above ~0.6 as temperature decreases and also as atmospheric pCO_2 increases above the "present" value (~320 ppmv at the time of the Broecker and Takahashi (1966) observations; rising toward 400 ppmv now). Cold water both at the ocean surface at high latitudes and in the cold, aphotic zone below the ocean surface mixed layer, therefore, has Ψ values higher than 0.6. Frankignoulle et al. (1994) used the notation "Ψ" for this exchange:reaction ratio, a notation I follow for the remainder of this analysis.

Egleston et al. (2010) independently confirmed the Frankignoulle et al. (1994) results and pointed out the relationship between the so-called "Revelle Factor" and Ψ. The Revelle factor measures the fractional rise in the pCO_2 of seawater relative to the fractional rise in the TCO_2 content seawater in gaseous equilibrium with the atmosphere (see Revelle and Suess 1957; Sundquist et al. 1979). This factor has a contemporary value near 8 in warm surface seawater and increases to about 14 in cold surface seawater. Barker et al. (2003) made future predictions of CO_2 gas evasion to be expected from $CaCO_3$ production as surface ocean Ψ rises to 0.76 (the value they predicted for about the year 2100).

The Ψ notation has led me to re-write Eq. 1 into a more general form, as follows:

$$Ca^{2+} + (1 + \Psi)HCO_3^- + (1 - \Psi)OH^- = CaCO_3 + \Psi CO_2 + H_2O \quad (3)$$

Smith and Veeh (1989) explicitly suggested a mass-balance linkage between $CaCO_3$ production and organic production in long residence time systems. We noted that, absent such a linkage, either net $CaCO_3$ reactions or net organic carbon reactions would quickly drive seawater properties such as pH, pCO_2, and calcite (and aragonite) saturation state well away from starting conditions. In the presence of such a linkage, these variables are retained at nearly constant values.

This observation leads to the tentative conclusion that an equation such as Eq. 3 might be further modified to link $CaCO_3$ and organic C metabolism in confined calcifying ecosystems:

$$Ca^{2+} + (1 + \Psi)HCO_3^- + (1 - \Psi)OH^- = CaCO_3 + \Psi(CH_2O + O_2) \quad (4)$$

That is, net $CaCO_3$ and organic C fluxes in confined systems might approximately compensate one another, with little or no net CO_2 gas flux. This equation appears conceptually useful in well-mixed, unstratified, hydrographically confined, shallow calcifying systems with long water residence time and relatively simple internal gradients of water composition; the equation is of lesser direct utility in vertically stratified systems such as the open ocean.

In shallow, vertically well-mixed systems with residence times of many days, the day-night effect of organic production and respiration is averaged out to a value near 0. Spatial locations of organic production and respiration (e.g., coral-algal communities, v. bare sediments), as well as any local $CaCO_3$ dissolution that might offset some of the $CaCO_3$ production, are indistinguishable with respect to water composition within such systems because of water mixing. The bulk TCO_2 signal that remains in the water is adequately represented by something like Eq. 3, the combined effect of $CaCO_3$ precipitation and CO_2 gas evasion with small or insignificant contribution of organic metabolism to the signal.

Net ecosystem $CaCO_3$ reactions are represented by both forward and reverse reactions like either Eq. 3 or 4. If the precipitation and dissolution reactions occur with Ψ having the same value for each, then net air-sea CO_2 gas flux is determined simply by the difference between the amount of $CaCO_3$ precipitated and the amount dissolved. If, however, precipitation and dissolution were to occur in separate water masses with differing values of Ψ, then the masses of $CaCO_3$ reacting on the two sides of the equation would no longer be the sole determinants of net CO_2 flux. If, for example, identical masses of $CaCO_3$ are precipitated and dissolved at different Ψ values, the net CO_2 gas flux will be determined by the difference in the value of Ψ. Differences of this sort would be expected in vertically stratified systems.

The open (pelagic) ocean is just such a stratified system. Both primary production and respiration obviously occur in the upper ocean. But, as stated in the introduction, a relatively large proportion of organic C production (as a global average, about 20% of net primary production) is exported from the surface ocean by particle fallout. That is, the upper ocean is a large net producer and exporter of organic matter.

Virtually all of that exported organic C is respired in the water column below the photic zone, as evidenced by the low organic C accumulation rates even on the surface of most oceanic sediments. There is a clear spatial separation between the sites of net organic C production and respiration in the water column, with the integrated water column net organic metabolism near 0. The respired CO_2 in the water column out of immediate contact with the atmosphere and light raises pCO_2 in the aphotic zone and has a significant impact on $CaCO_3$ reactions there, by inducing $CaCO_3$ dissolution. Therefore Eq. 4 may have conceptual merit, but its application in the vertically stratified world ocean is complicated by this vertical separation between major sites for production and respiration (as well as net $CaCO_3$ precipitation and dissolution).

In the scientific literature cited to this point, Ψ has been discussed almost entirely in terms of gas equilibration with the atmosphere. A complication arises with Ψ, its variation in the water column as a function of temperature and pCO_2, and the role of this variable Ψ with respect to water column $CaCO_3$ reactions and CO_2 fluxes. Smith and Gattuso (2011) recently pointed out that the flux ratio represented by Ψ applies equally to water that is not exchanging CO_2 with the atmosphere. If the water is not equilibrating with the atmosphere, the CO_2 released by the forward reaction of Eq. 3 remains as dissolved, undissociated CO_2 in the water, rather than exchanging with the atmosphere. There is a concomitant increase in the pCO_2 of that water.

Smith and Gattuso (2011) demonstrated that seawater along most of a north-south transect through the central Pacific Ocean has surface Ψ values near 0.6, whereas water deeper than a few hundred meters has values of about 0.9. This rise reflects the combined effects of (a) a rise in seawater pCO_2 values from near equilibrium with the atmosphere to values greater than 1000 µatm near a water depth of 1000 m as organic carbon decomposes and TCO_2 accumulates in the water below the mixed layer, and (b) a decrease in water temperature from near-atmospheric temperatures at the ocean surface (global mean ~16°C; http://www.ncdc.noaa.gov/cmb-faq/anomalies.php; last accessed 2 Mar 2012) to deep ocean values near 0°C.

Smith and Gattuso (2011) cited summary data from Milliman and Droxler (1996) that $CaCO_3$ precipitation by both planktonic and benthic processes totals about 90×10^{12} mol y^{-1} in the world ocean, while accumulation totals about 30×10^{12} mol y^{-1}. The difference between production and accumulation implies that 60×10^{12} mol y^{-1} dissolves.

Milliman and Droxler and Milliman et al. (1999) concluded that most of that $CaCO_3$ dissolution occurs in the water column above the calcite lysocline. This conclusion and other pieces of evidence for "hyper-lysocline dissolution" cited by Milliman et al. (1999) contrast with the long-held view that $CaCO_3$ dissolution occurs primarily below the calcite lysocline (see also Smith and Gattuso [2011] and recent citations therein).

Smith and Gattuso (2011) used data from the Central Pacific Ocean to demonstrate that present precipitation of $CaCO_3$ largely occurs in that portion of the water column with Ψ ~0.6; dissolution occurs in the region with Ψ ~0.9. Smith and Gattuso (2011) further argued that if this pattern for the central Pacific Ocean typifies the world ocean, then net CO_2 flux from water-column $CaCO_3$ reactions predicted from Eq. 1 is 0. Under these conditions of Ψ and of $CaCO_3$ precipitation and dissolution, net $CaCO_3$ precipitation would be neither a net source nor a net sink of atmospheric CO_2. We concluded from this approximation for the central Pacific Ocean that Eq. 1 is not a quantitatively accurate representation of CO_2 flux associated with the oceanic $CaCO_3$ cycle.

In reflecting on the conclusions we derived in Smith and Gattuso (2011), I decided that implications with respect to expected air-sea CO_2 flux associated with oceanic $CaCO_3$ reactions were sufficiently important to merit a more comprehensive quantitative analysis. The analysis has led me to some interesting and surprising observations. That analysis, as presented here, strives to provide a quantitatively accurate estimation of the role of Ψ in the contemporary oceanic carbon budget, using a large repository of high-precision oceanic data collected by scientists from many institutions over the past two decades.

That analysis points out the importance of benthic versus pelagic $CaCO_3$ reactions with respect to CO_2 gas flux. Despite the vertical separation between sites of net $CaCO_3$ precipitation and net dissolution, the sites and processes are inextricably linked. This linkage is then explored in the context of the contemporary ocean (including ongoing anthropogenic effects); changing shallow sea floor area over the past 120,000 years (the most recent glacial-interglacial cycle); and aspects of $CaCO_3$-related CO_2 flux over Phanerozoic time (~550 million years).

Chapter 3. Materials and Methods

Water chemistry data for the world oceans were downloaded from the World Ocean Database 2009 (WOD09; http://www.nodc.noaa.gov/OC5/WOD09/pr_wod09.html; last accessed 2 Mar 2012). The bottle data downloaded for analysis included salinity, temperature, total alkalinity (TA), total CO_2 (TCO_2), phosphate and silicate data. Any two variables related to the aqueous CO_2 system, along with temperature, pressure, salinity, phosphate, and silicate, comprise the minimum data set required to calculate high-precision values of pCO_2 and $CaCO_3$ saturation state (Ω; here only calcite saturation state, Ω_c, is explicitly reported) (Dickson et al. 2007). The phosphate and silicate data are also used in the equilibrium calculations. The nutrient contributions to TA can be significant through the water column, which typically has large vertical variations in nutrients.

Ψ was calculated as described by Smith and Gattuso (2011), as follows. The calculation procedure simulates the DIC change that occurs if a specified amount (here, 100 µmol kg^{-1}) of $CaCO_3$ were precipitated from water of known TA and TCO_2, and then returned to that water's starting pCO_2. This amount of precipitation lowers TA by 200 µeq kg^{-1}. In qualitative accordance with Eq. 1, pCO_2 of the water rises with $CaCO_3$ precipitation; over time, the water returns to its starting pCO_2 by degassing (i.e., losing part of its TCO_2). That is, it adjusts to the conditions of Eq. 3.

Finally, the new, gas-equilibrated TCO_2 is calculated. The coefficient, Ψ, is then calculated from the changes in TCO_2 and TA: ($\Psi = [\Delta TCO_2 - \Delta TA/2]/[\Delta TA/2]$, where "Δ" represents concentration changes in response to the simulated $CaCO_3$ precipitation, CO_2 gas evasion, and gas re-equilibration back to the initial sample pCO_2 in accordance with Eq. 3). There is also a slight contribution of TA to variation of Ψ, so the calculations as performed here introduce a systematic error of < 0.01 in the calculated value of Ψ.

For modeling purposes in various parts of the analysis, Ψ is calculated as a function of a constant value of TA (2300 µeq kg^{-1}) and variable pCO_2. Salinity and temperature are held constant (35 and 20°C, respectively) for this calculation. The relationship between 200 and 3000 ppmv is well approximated by the following regression $\Psi = 1.1 - 5.26 \times pCO_2^{-0.451}$ (r^2 between Ψ calculated as in the previous paragraph and Ψ fitted to this equation = 0.99).

TA and TCO_2 were chosen as the "master" CO_2-system variables to download from WOD09, because these variables are now measured to high precision and accuracy on many modern oceanographic surveys of water chemistry. Graphic representations of property distributions for TCO_2 and TA in the water column use values normalized to a salinity of 35, to remove conservative variations associated with salinity variations. In the case of TA, the data used for graphic presentations are also adjusted to remove nutrient alkalinity contributions from phosphate and silicate. Actual calculations of Ψ relied on the unadjusted TA values, because the programs used for the analysis of the CO_2 system automatically correct for nutrients and salinity (as well as pressure and temperature).

The data analyzed were restricted to data collected since 1990, deemed the most reliable period for high-precision TCO_2 and TA data (see Johnson et. al. 1998; Millero et al. 1998). A few samples were discarded because of obvious data transcription errors in the WOD09 database. With these restrictions, there were ~110,000 samples (bottles representing discrete water depths) from ~6,800 hydrographic stations.

The data were divided into the following 8 ocean provinces: (1) Gulf of Alaska (north of 45° N); (2, 3) North and South Pacific Ocean (45° N to 0°;(0° to 45° S, respectively); (4) Arctic Ocean (north of 55° N); (5, 6) North and South Atlantic Ocean (55° N to 0°; 0° to 45° S, respectively); (7) Indian Ocean (30° N to 45° S); and (8) Antarctic Ocean (south of 45° S).

The latitudinal boundaries of these provinces were chosen to emphasize biogeochemically useful variations in composition, rather than conforming to geopolitically recognized oceanic regions.

To describe regional oceanic conditions with minimal contributions from locally generated "environmental noise," stations from areas with water depths shallower than 150 m or within 100 km of the coast were excluded from the dataset (total exclusions, 6783 samples; 629 stations). Fig. 1 and Table 1 summarize the geographic distribution of the data used.

Files with the original data and summarized by ocean province (including the "coastal stations" that were excluded from the calculations presented here) may be found at http://www.aslo.org/books/smith_s/smith_s_parsing/completedataset.xlsx.

Calculations and initial data exploration were carried out using Ocean Data View (http://odv.awi.de; last accessed 2 Mar 2012). Reiner Schlitzer, the developer of ODV, kindly provided a pre-release version of ODV 4.3.11.2. That and subsequent versions of ODV include calculations of CO_2-related variables. ODV output was used

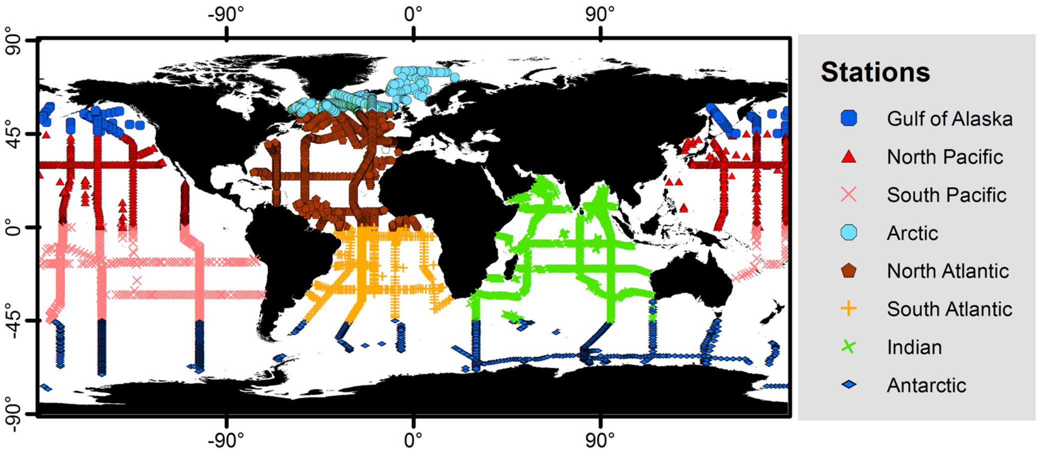

Fig. 1. World map, showing WOD09 station locations used, as well as division of the data by oceanic province.

Table 1. WOD09 data extracted for the period 1990-2010, and a summary of the data used in the present analysis. Oceanic provinces and station locations are shown in Fig. 1.

Oceanic province	Bottle samples	Hydrographic stations
Gulf of Alaska	2429	140
North Pacific	19,088	1175
South Pacific	14,106	671
Arctic	4648	449
North Atlantic	19,634	1299
South Atlantic	9215	486
Indian	21,146	1211
Antarctic	13,061	751
TOTAL	103,327	6182

(according to the rules given above) to calculate Ψ. CO_2-related calculations from ODV were checked against the widely used CO2SYS program developed by Lewis and Wallace (1998).

Ψ is accorded particular attention in this analysis. Maps of Ψ distribution in the global ocean within 3 depth layers, were prepared with ArcMap. Data from individual bottles were used with Inverse Distance Weighting (in 2° "squares" of latitude/longitude). For each map, the continents are masked out in black; coastal areas (as defined above) and areas shallower than the depth used for each map (extracted from ETOPO1; http://www.ngdc.noaa.gov/mgg/global/global.html; last accessed 2 Mar 2012) are masked out in white. Individual station locations are shown by dots on each map.

The sea level curve for the past 120,000 years was extracted from supporting online material from Miller et al. (2005). Elevation data for calculating changing shallow sea floor area over this time were extracted from ETOPO1. The 1 arc-minute pixels of water depth in ETOPO1 were reprojected to cylindrical equal area (1.479 km pixel size) in ArcMap for calculations of areas within depth classes.

Atmospheric CO_2 data for the past 120,000 years (Holocene Epoch) were reconstructed from the online data link reported in Lüthi et al. (2008). Modeled CO_2 data for the past 570 million years (Phanerozoic Era and latest portion of the Pre-Cambrian) were extracted from figures in Berner (2004a).

Chapter 4. Results

The first subsection of this chapter is *Analysis of CO_2-related variables in the world oceans*. With this background information, calculations of CO_2 fluxes associated with $CaCO_3$ production and dissolution are presented, along with the global ocean $CaCO_3$ budget analysis used for the calculations (see *CaCO3-mediated gas flux in pelagic versus benthic sub-systems of the ocean*). The calculations are split between benthic (primarily shallow-water) and planktonic sub-systems of the contemporary world ocean. Atmospheric CO_2 concentrations are presented over geological time, and it is argued that these concentrations are reasonable proxies of pCO_2 in the surface ocean (see *Variation of atmospheric CO_2 over time*). Estimations of CO_2 flux are then made for the increasingly acidified, "post-modern," high-CO_2 world (atmospheric pCO_2 = 500 ppmv) [see *Effect of Ψ on CO_2 flux in the post-modern (increasingly acidified) world ocean*]. Simulations are then presented for the past 120,000 years to evaluate the significance, for the carbon budget, of the changing area of shallow sea floor on the role of $CaCO_3$ reactions within the benthic sub-system (see *CaCO3-mediated gas flux with glacial-interglacial variations in sea level*). Finally, there is a discussion of how variation of Ψ over the past 570 million years may have affected the oceanic $CaCO_3$ cycle with respect to atmospheric CO_2 flux (see Variation of Ψ over Phanerozoic time).

Analysis of CO_2-related variables in the world oceans

Figs. 2-6 summarize the major patterns of vertical data distribution discussed in the present analysis. The figures are laid out in a manner topologically approximating the geographic positions of the oceanic provinces. Data were summarized for each province as follows.

More than half of the individual bottle samples used occur in the upper 1000 m of the water column, so profile details are greater in that region. Properties were averaged into 50-m (depth) bins over the upper 1000 m of the water column. For the water column between 1000 and 5500 m, 250-m bins were used. The few samples deeper than 5500 m (typically to near 6000 m) were averaged for a "near-bottom" sample. Bin-averaging in this manner adequately describes vertical gradients of water column properties, because most of the vertical variation in the relevant properties occurs in the upper 1000 m of the water column.

Temperature profiles (Fig. 2) show useful patterns with respect to the reasoning for choosing the province boundaries. The three high-latitude provinces (Gulf of Alaska, Arctic, Antarctic) show average surface temperatures below 10°C, and little temperature variation with depth. By contrast, the five lower latitude provinces (North and South

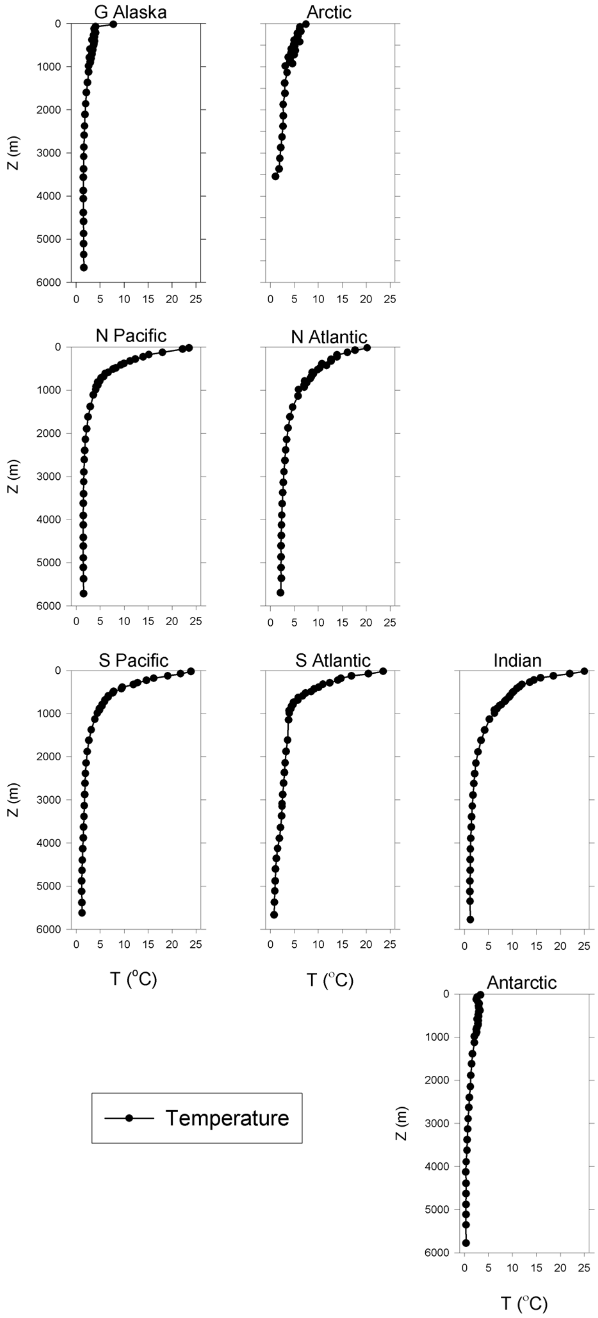

Fig. 2. Vertical profiles of temperature for the 8 oceanic provinces. Note that the Gulf of Alaska, Arctic, and Antarctic provinces all have surface temperatures below 10°C. The low latitude provinces have average surface temperatures well above 10°C.

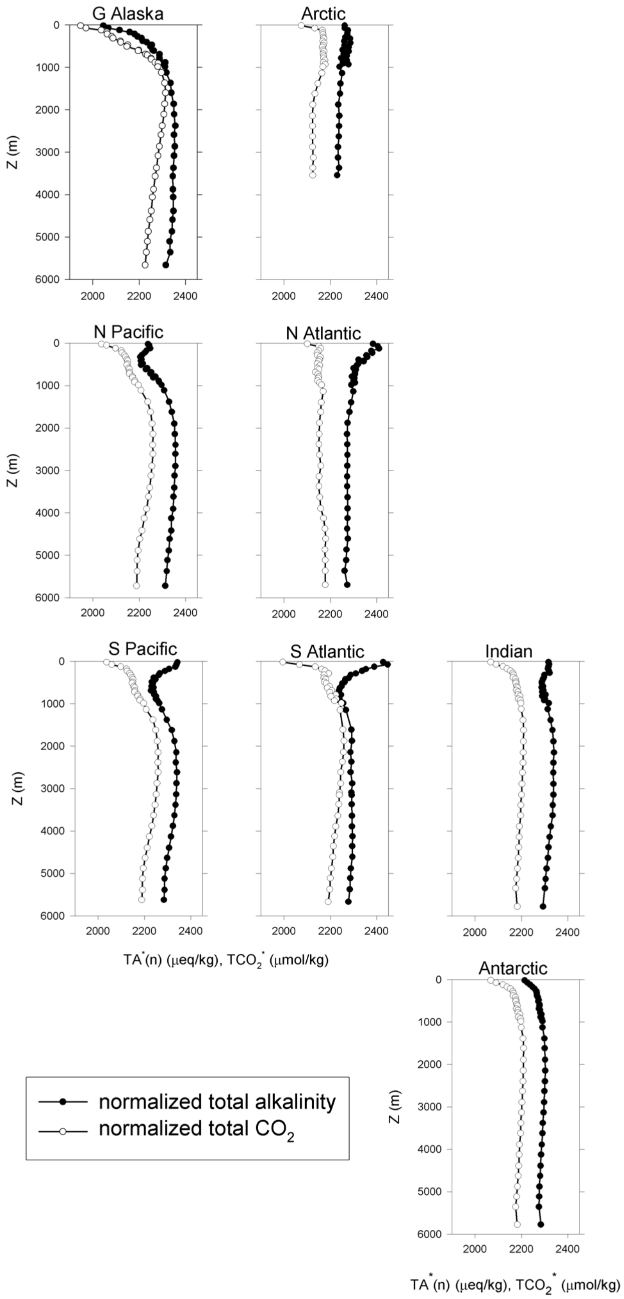

Fig. 3. Vertical profiles of TA*(n) and TCO_2* for the 8 oceanic provinces. In general, for the low-latitude provinces TCO_2 begins to rise, whereas TA*(n) decreases until deeper in the water column. TA*(n) does not vary a great deal below 1000 m.

Pacific, North and South Atlantic, Indian) all show average surface temperatures well above 10°C, and well-developed thermoclines. At the scale of the figures and at the 50-m resolution of bins in the upper water column, the near-constant mixed layer temperatures are not obvious in the profiles.

Total alkalinity [normalized in Fig. 3, to a salinity of 35 and adjusted to remove phosphate and silicate contributions, $TA^*(n)$] diminishes immediately below the surface waters in the lower latitude provinces. This decrease represents TA uptake into $CaCO_3$, but without the rapid mixing and homogenizing that occurs in the surface mixed layer. Of the lower latitude provinces, all except the North Atlantic show a rise in $TA^*(n)$, primarily between about 500 and 1000 m. Thus, the lower latitude provinces generally show evidence of upper water column $CaCO_3$ precipitation (above 500 m), and of dissolution somewhat deeper in the water column (primarily in the interval between 500 and 1000 m).

Normalized total CO_2 (TCO_2^*) profiles are also shown on Fig. 3. The lower latitude provinces demonstrate that TCO_2^* below 50 m rises at shallower depths than $TA^*(n)$, as organic particles exit the photic zone and decompose.

The depth range of rapidly rising $TA^*(n)$ is generally well above the calcite lysocline (Fig. 4; the depth below which $\Omega_C = 1.0$). In the Pacific, $\Omega_C = 1.0$ occurs near 1000 m, whereas the lysocline is substantially deeper in the Atlantic and Indian Oceans. These lysocline depths relative to depths of rising $TA^*(n)$ support growing evidence that much (apparently most) $CaCO_3$ dissolution in the ocean occurs in waters that are supersaturated with respect to calcite. This phenomenon is probably the result of dissolution associated with organic carbon decomposition in microlayers surrounding sedimenting $CaCO_3$ particles (e.g., Martin and Sayles 1996).

Fig. 5 summarizes the water column distribution of pCO_2. Surface water pCO_2 is typically near atmospheric CO_2, with the exact value set by a combination of upward transport (by advection or mixing) of higher-PCO_2 water from below the mixed layer, air-sea gas exchange, and photosynthetic uptake of CO_2 in the photic zone. The rise of pCO_2 with increasing depth immediately below the mixed layer represents oxidation of organic matter, whereas the decrease in pCO_2 below about 800-1000 m at least partially represents dissolution of $CaCO_3$, with consequent diminution of both free CO_2 and pCO_2, and increase in both $TA^*(n)$ and TCO_2^* below that depth. The rapid diminution of pCO_2 in this depth range well above the calcite lysocline is further evidence of $CaCO_3$ "hyper-lysocline dissolution."

Finally, consider the vertical distributions of Ψ (Fig. 6). The lower latitude provinces, where it can be inferred that most $CaCO_3$ precipitation occurs, have surface water Ψ near 0.6, with a sharp rise down to depths of 500-1000 m, then nearly constant Ψ values at greater depths.

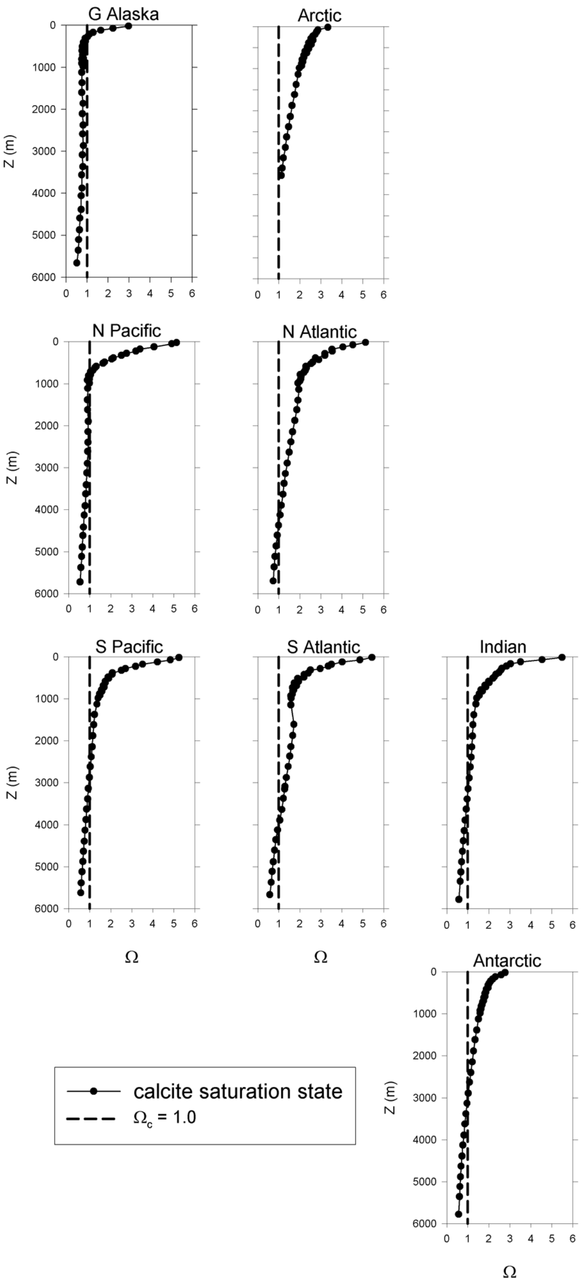

Fig. 4. Vertical profiles of Ω_c for the 8 oceanic provinces.

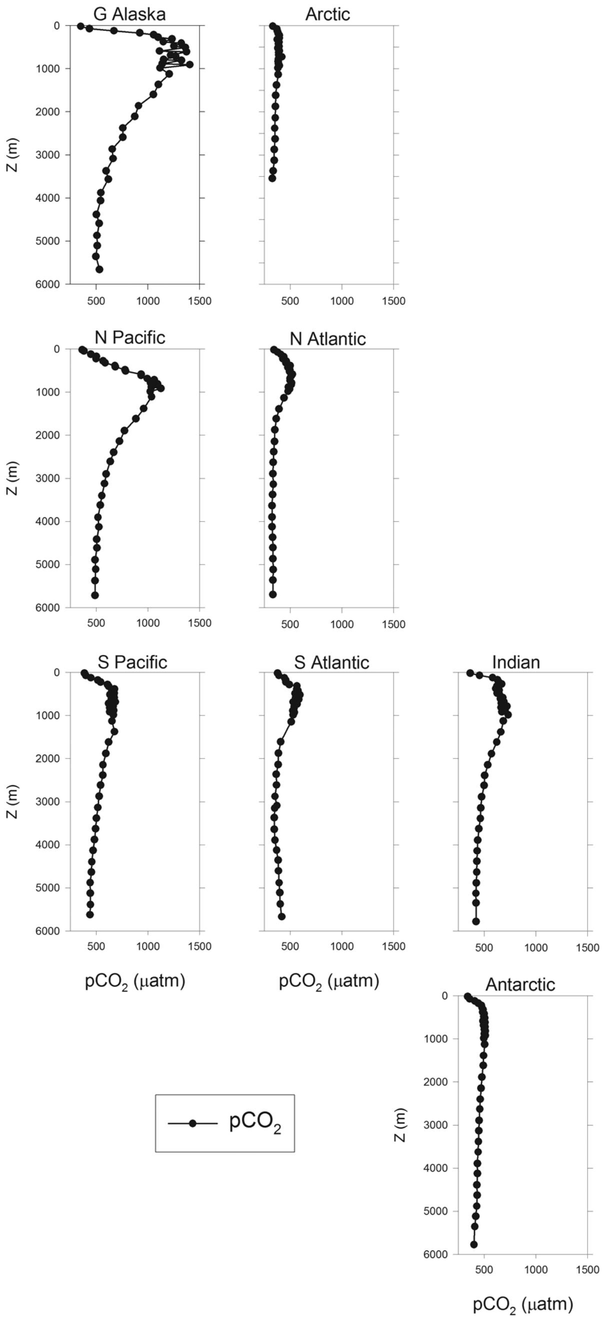

Fig. 5. Vertical profiles of pCO_2 for the 8 oceanic provinces. The pCO_2 decrease below 500-1000 m reflects uptake of gaseous CO_2 associated with $CaCO_3$ dissolution. This generally occurs above the depth at which Ωc reaches a value of 1.0 (Fig. 4).

Because Ψ is key to subsequent analyses of CO_2 gas flux associated with $CaCO_3$ reactions, Fig. 7 is included to show the geographic distribution of this variable approximately in the mixed layer (0-50 m), approximately at the depth of maximum Ψ (900-1100 m), and at depths > 3000 m. Several interesting trends emerge from those distribution maps.

Mixed layer values for Ψ show a distinct latitudinal distribution across the oceans, with a secondary upwelling-related trend. In general, Ψ is near 0.6 at latitudes lower than 45° (N and S), with higher Ψ values at latitudes above 45°. The upwelling trend in mixed-layer Ψ is particularly evident in the eastern equatorial Pacific Ocean, with slight elevations of Ψ there and in other regions of substantial upwelling.

In contrast with the shallow-water trends for Ψ, the primary pattern in deeper water is most distinctive by ocean province. The North Pacific and, to lesser extent, the Indian Oceans show the highest values for Ψ near 1000 m; at this depth, the North Atlantic shows the lowest Ψ values; the Antarctic is intermediate. The variation of Ψ in these intermediate waters is consistent with variation of deep ocean ventilation times (e.g., England 1995). Ψ values in water deeper than 3000 m vary less than at the intermediate depth, and are very slightly lower than they are near 1000 m.

Table 2 provides a summary of surface and deeper water Ψ for profiles of each of the provinces. The mean values for surface and deeper water Ψ are not weighted by the areas or volumes of the ocean provinces, because a more meaningful weighting would be by relative $CaCO_3$ reactions (production, dissolution). There is no immediately obvious way to accomplish that weighting with available information at the present time. To do so would require actual spatial resolution of the variations in rates of $CaCO_3$ reactions (production, dissolution), rather than broad averages by community type. One way to achieve that resolution might be to use spatially explicit models of those processes.

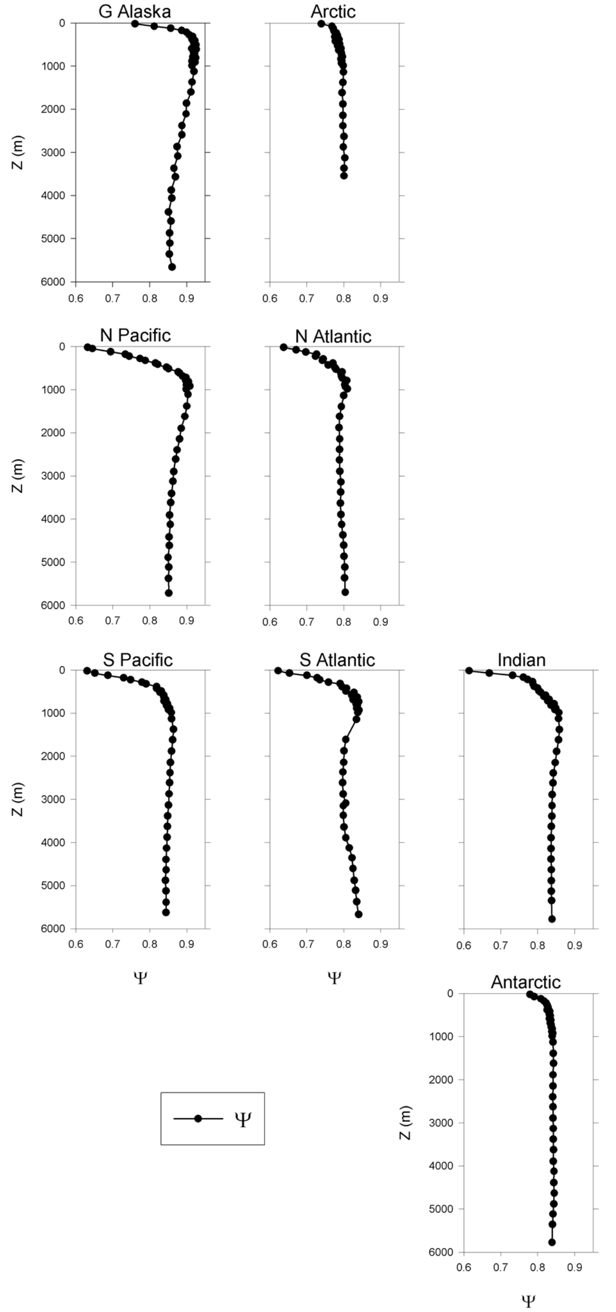

Fig. 6. Vertical profiles of Ψ for the 8 oceanic provinces. Note the surface ocean values and the approach (by ~1000 m) to nearly constant deep ocean values.

Near-surface, low-latitude water, where most $CaCO_3$ production apparently occurs, has a mean $\Psi = 0.63$ (SE = 0.006); high-latitude surface water Ψ averages 0.77 ± 0.009, but this water is apparently relatively insignificant with respect to $CaCO_3$ fluxes. Deeper water (the site of most dissolution) has $\Psi = 0.85$, with little difference between the low-latitude and high-latitude provinces (0.85 ± 0.001, 0.84 ± 0.001, respectively). Very similar average values are obtained from the Ψ maps. The important points to note are (a) $CaCO_3$ production apparently largely occurs at $\Psi \cong 0.63$ and (b) most dissolution occurs at $\Psi \cong 0.85$. There is, thus, about a 35% difference in Ψ between sites of major $CaCO_3$ production and dissolution.

$CaCO_3$-mediated gas flux in pelagic versus benthic sub-systems of the ocean

The contemporary distribution of Ψ (Table 2) can be used in concert with a simple box-model presentation of the global $CaCO_3$ budget. The box model includes surface and deep ocean boxes (where chemical reactions occur) and sediment boxes (where accumulation occurs).

The $CaCO_3$ budget used in the box model and the references leading to that budget are summarized in Table 3. The data in the table demonstrate some important characteristics. First, there are substantial differences within the columns (i.e., categories) of estimated fluxes. Second, the differences between production and accumulation define the estimated dissolution; this flux property is important in defining the net air-sea CO_2 flux. Third, despite the variations among the estimates of each flux, the "comments" column demonstrates that the apparently differing estimates tend to be readily explained and to converge toward reasonable consensus estimates of

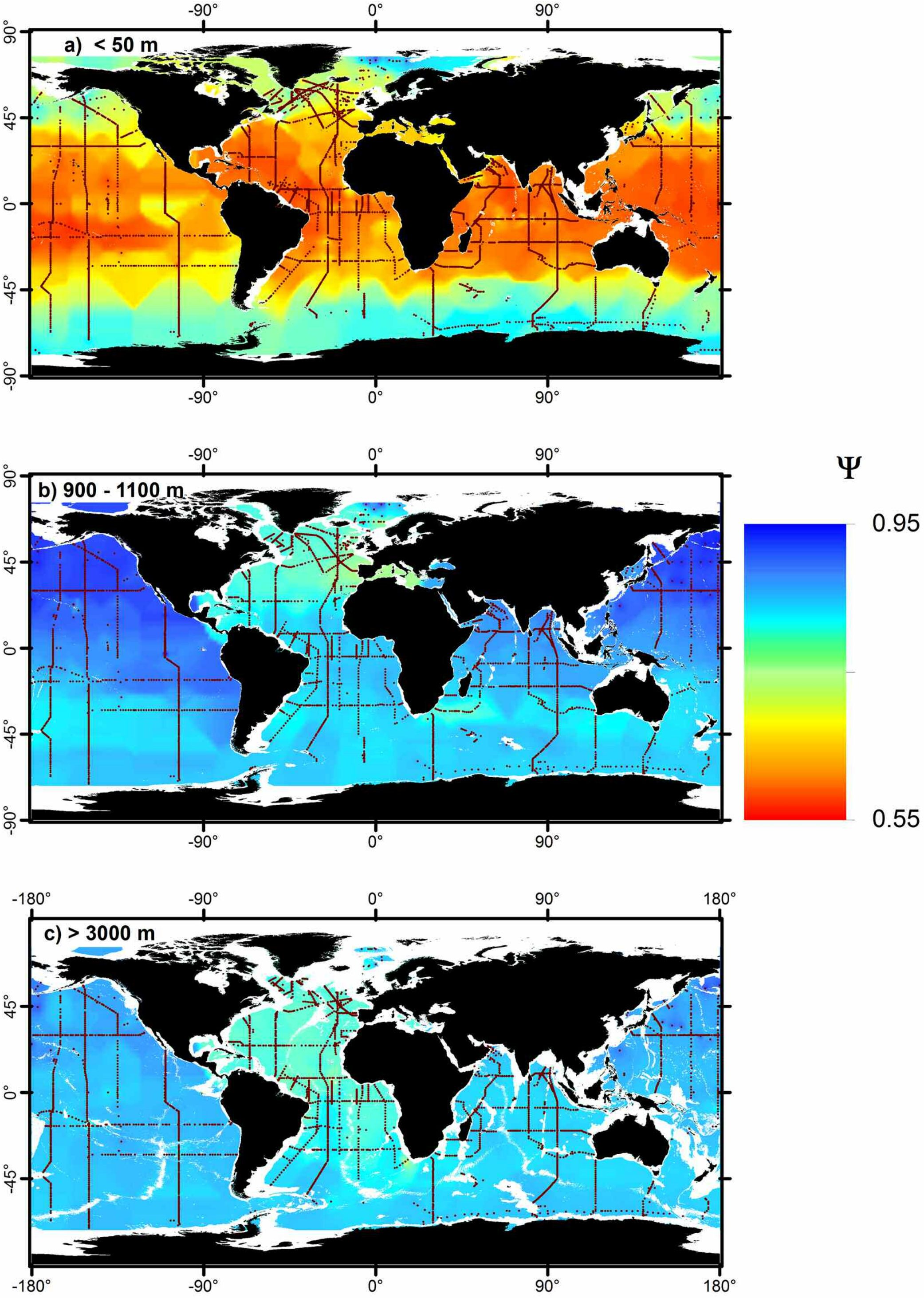

Fig. 7. Maps showing Ψ at three key depths: (a) water between 0 and 50 m deep, approximately the mixed layer; (b) water 900–1100 m deep, approximately the maximum Ψ values; (c) water > 3000 m deep.

both production and accumulation fluxes. I use the "round number best estimates" presented as the last row in that table; those estimates differ insignificantly from the budget presented by Milliman and Droxler (1996).

Table 2. Ψ in surface water and maximum water-column Ψ in the oceanic provinces. The "lower latitude provinces" are North and South Pacific, North and South Atlantic, and Indian. The "higher latitude provinces" are Gulf of Alaska, Arctic, and Antarctic.

Oceanic Province	Ψ_{surf}	Ψ_{max}
Gulf of Alaska	0.76	0.92
North Pacific	0.63	0.90
South Pacific	0.63	0.86
Arctic	0.74	0.80
North Atlantic	0.64	0.80
South Atlantic	0.62	0.84
Indian	0.61	0.85
Antarctic	0.78	0.84
Profile averages		
All provinces $\bar{X}$ ±SE	0.66 ± 0.008	0.85 ± 0.001
Lower latitude $\bar{X}$ ±SE	0.63 ± 0.006	0.84 ± 0.001
Higher latitude $\bar{X}$ ±SE	0.77 ± 0.009	0.85 ± 0.001

Other budgets that are not as fully laid out as the Table 3 budgets can be found in the literature. Some deal only with specific type of systems (e.g., reefs) or even biotic components within systems (e.g., corals, calcifying algae, mollusks, echinoderms, foraminifera) or with specific locations or seasons. Some are not presented or defended in much detail. The Milliman and Droxler (1996) budget, which is the underlying basis for the "round number best estimates" budget in Table 3, represents the last (to date) in a series of global budget estimates which John Milliman began assembling in 1974. Each iteration has provided thoughtful explanations for revising specific aspects of the preceding estimates. For example, earlier global budgets and many local budgets of coral reef accumulation mixed contemporary estimates of production with reef borehole data that included erosional or nondepositional intervals in the total accretion rates.

The Milliman and Droxler budget has gained the imprimatur of being "endorsed" by a committee of prominent geoscientists (Iglesias-Rodriguez et al. 2002) as being the best we presently have. It is, of course, possible (even probable), that quantitatively significant flaws will emerge in the evolving budget presented in Table 3; certainly the amount of data available remains sparse. The point, however, is not the ultimate accuracy of that budget. Rather, the budget provides a basis for evaluating how pelagic and benthic components of oceanic $CaCO_3$ reactions interact and structure the role of global ocean C flux with respect to air-sea interactions of CO_2 flux.

Of particular utility to the present study, the approach which Milliman has used in his estimates provides explicit estimates of production, accumulation, and—by difference—an estimate of dissolution. Whereas there undoubtedly will continue to be revisions of the specific numbers in this budget, its underlying structure and conclusions about the approximate magnitudes of production, accumulation, and dissolution within the pelagic and benthic realms seem unlikely to change sufficiently to invalidate use of this budget to demonstrate the role of oceanic $CaCO_3$ reactions in the global carbon cycle.

For purposes of the present analysis, I illustrate the box model split between surface and deep water boxes, and between pelagic and benthic sub-systems (Fig. 8). These splits may be considered a simplified one-dimensional approach that distinguishes Ψ between the low-latitude surface (predominantly $CaCO_3$ producing) and deep (predominantly $CaCO_3$ dissolving) portions of the oceanic water column. The major benthic contribution to the budget is by neritic (shallow-water) communities in the low-latitude provinces, with only a minor contribution by slope and deeper benthic calcifying communities (analysis and discussion of Milliman and Droxler 1996).

Benthic $CaCO_3$ production is dominated by coral reefs and related shallow tropical communities, but also includes production by shallow-water communities at higher latitudes (See Supplementary Material—*Calcifying Habitats* http://www.aslo.org/books/smith_s/smith_s_parsing/smith_s_envirofigures.pdf). Both the tropical and higher latitude benthic calcifying communities include a wide variety of calcifying taxa. Benthic production and accumulation include calcite (both low-Mg and higher-Mg calcite), as well as aragonite. Pelagic production is dominated by planktonic forms: coccolithophorids, planktonic foraminifera, and pteropods. Most of the aragonitic pteropod shells dissolve without accumulation, so calcitic coccolith and foram muds dominate accumulation arising from

Table 3. Summary of budgets that were used to derive the "round number best estimate budgets" for the present study. [See also Iglesias-Rodriguez et al. (2002) for a general review and "community endorsement" of Milliman and Droxler (1996) budget].

$CaCO_3$ fluxes (10^{12} mol y^{-1})	**Pelagic**		**Benthic**		**Total**		
Reference	**prod.**	**accum.**	**prod.**	**accum.**	**prod.**	**accum.**	**Comments**
Li et al. (1969)	60	12					Vertical distribution of alkalinity.
Milliman (1974)		11		12		23	Reef accumulation based on drill core data, including glacial periods of little or no accumulation, or erosion.
Morse, and Mackenzie (1990)	72	12	14	5	86	17	Reef production, accumulation based on drill core data; see previous entry.
Milliman (1993)	24	11	30	23	54	34	Pelagic production based on sediment flux at 1000 m; much has already dissolved. See Milliman and Droxler (1996, below).
Wollast (1994)	65	12	29	21	94	33	Revises Morse and Mackenzie (1990) benthic production upward with contemporaneous flux data for reefs. Mackenzie et al. (2005) adopt this budget.
Milliman and Droxler (1996)	60	11	30	21	90	32	Revises pelagic production upward to reflect surface production, rather than 1000 m sediment fallout.
Catubig et al (1998)		9					Most comprehensive estimate of pelagic accumulation.
Lee (2001)					92		Hydrographic and alkalinity-based estimate of production.
Mean	55	11	26	16	83	28	Pelagic production noisy because of Milliman (1993) underestimate. Benthic production noisy because of Morse and Mackenzie (1990) and Milliman (1993) use of reef drill core estimates including both glacial interglacial data; see previous discussion above.
Median	63	11	30	21	90	32	
Standard deviation	21	1	8	8	17	7	
This paper	60	10	30	20	90	30	"Round-number" best estimates.

planktonic production. Milliman (1974) provides a useful summary of common calcifying taxa of both pelagic and benthic organisms, including a discussion of the mineralogies of these organisms. Papers in Gattuso and Hansson (2011) discuss various effects of oceanic chemistry on the biogenic calcification process.

The results from separating the pelagic and benthic sub-systems are dramatic. Only a small proportion (~1/6) of the pelagic production accumulates in the sediments; the remainder dissolves. By contrast, most (~2/3) of the benthic production accumulates in the sediments, rather than dissolving. These general differences between production and accumulation of $CaCO_3$ in the pelagic and benthic realms of the ocean have long been recognized (e.g., Milliman 1974).

The analysis presented here explores the consequences of these differences in production, dissolution, and accumulation with respect to net gas flux in an ocean characterized by vertically variable Ψ. Pelagic fluxes (production in surface waters, downward transport by fallout from the surface layer, and dissolution in water deeper than ~500 m) result in net CO_2 gas influx into the ocean, even though $CaCO_3$ production exceeds dissolution. This result reflects the vertical variation of Ψ. Pelagic $CaCO_3$ precipitation occurs at $\Psi \sim 0.63$, driving off CO_2

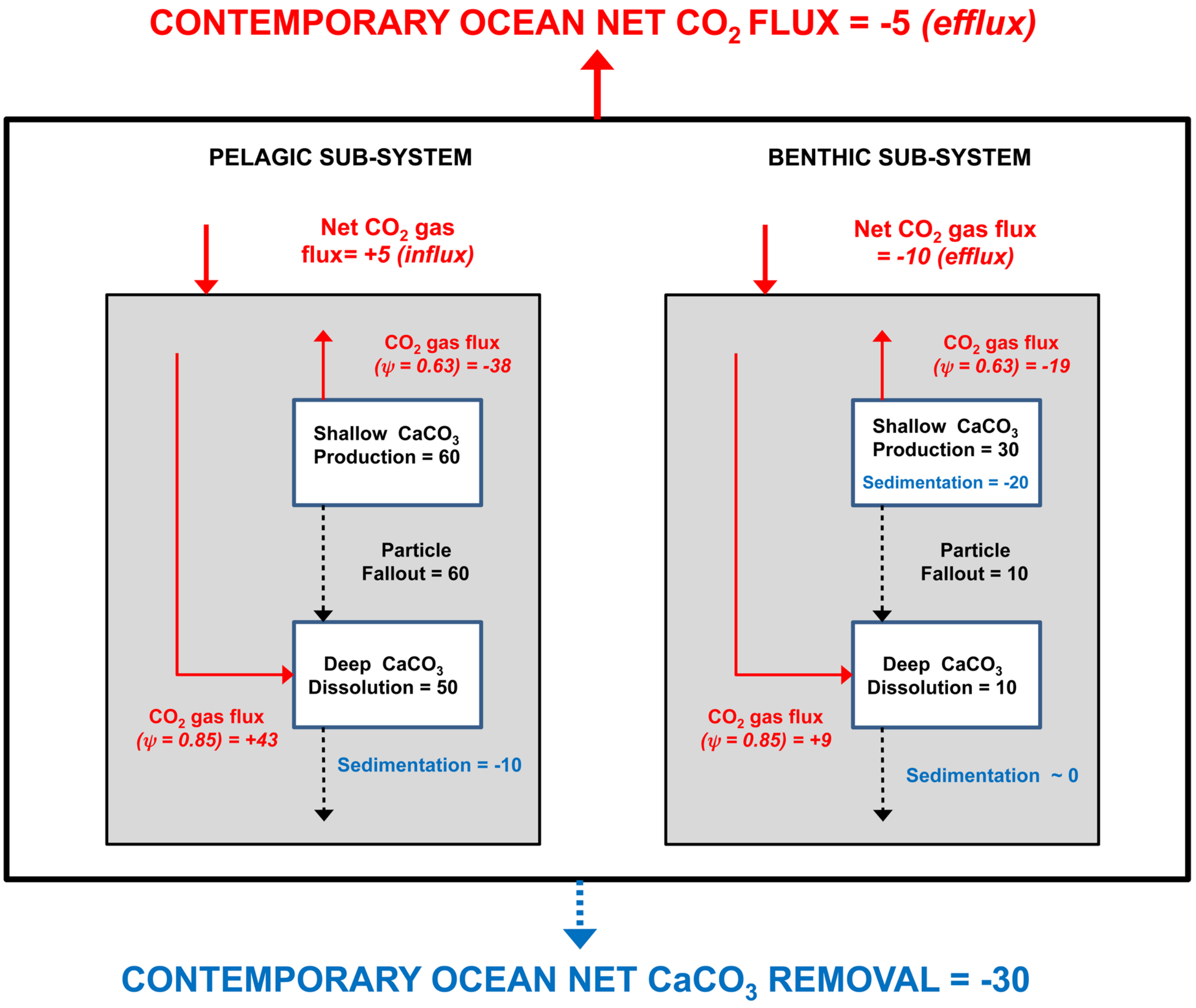

Fig. 8. Contemporary global ocean $CaCO_3$ budget, split into pelagic and benthic sub-systems. Fluxes are in units of 10^{12} mol y^{-1}. The combined (net) CO_2 gas flux associated with oceanic $CaCO_3$ production and dissolution is an efflux of 5 × 10^{12} mol y^{-1}.

accordingly. Most (~5/6) of the $CaCO_3$ production dissolves in water with Ψ ~ 0.85. The difference between $CaCO_3$ production at a relatively low value of Ψ and dissolution at a higher value of Ψ causes net absorption of gaseous CO_2.

This assertion deserves explicit explanation via a simple algebraic example. Let us express the amount of precipitation as 1 and dissolution as 5/6. Then, 1 × 0.63 = 0.63 (precipitation-induced gas release in surface waters); 5/6 × 0.85 = 0.71 (dissolution-induced gas absorption in deeper waters). Net = (Absorption – Release) = (0.71 – 0.63) = + 0.08. There is net absorption, even though there is also a small amount of net $CaCO_3$ production (and sediment accumulation).

The CO_2 that is released in the mixed layer is quickly transferred to the atmosphere by air-sea gas equilibration. CO_2 absorbed in the water column below the mixed layer is scavenged from free CO_2 released into the water column by organic matter oxidation below the mixed layer. This scavenging reduces the return flux of CO_2 from organic oxidation in the water column back to the surface and, eventually, the atmosphere. The scavenged CO_2 accumulates in deep water over the ventilation time of the deep ocean (ranging from decades in areas such as the North Atlantic and Antarctic to 500-1500 y in the Western Pacific; England 1995).

The benthic sub-system, in contrast with the pelagic sub-system, experiences relatively little dissolution at elevated values of Ψ, because most material accumulates near its production site. This result may be somewhat misleading, although I believe the estimated consequences with respect to CO_2 fluxes are robust. Several of the benthic $CaCO_3$ production data sets used by Milliman and Droxler (1996) were derived from alkalinity-based studies of reef and carbonate bank $CaCO_3$ production. Those estimates are, by their very nature, net production estimates, because they are based on local net changes in alkalinity. However, any fraction of gross production which is locally dissolved would undergo both production and dissolution (yielding net production) at a constant value of Ψ (0.63, according to the analysis presented here). Only the small proportion of benthic production that is moved to deep water before dissolution would be subjected to higher dissolution values of Ψ (0.85). Therefore the benthic sub-system production of $CaCO_3$ shows net gas evasion.

The combined global effect of the benthic and pelagic $CaCO_3$ fluxes, including the vertical variation in Ψ and the sites of $CaCO_3$ production and dissolution, may be summarized as follows. Contemporary values for the combined pelagic plus benthic ocean $CaCO_3$ reactions indicate some net flux of CO_2 gas to the atmosphere (Fig. 8). The global ocean net CO_2 gas efflux associated with this net oceanic accumulation of 30×10^{12} mol $CaCO_3$ y^{-1} is 5×10^{12} mol CO_2 y^{-1}. This flux is only 17% of the CO_2 efflux that would be predicted by the quantitative application of Eq. 1, a quantitatively dramatic departure from that equation.

Variation of atmospheric CO_2 over time

It has been recognized at least since the 1950s that atmospheric CO_2 variation over time is a sensitive recorder of processes in the global C cycle. The surface ocean is well mixed and in intimate contact with the atmosphere (e.g., Sigman and Boyle 2000). As a result, the atmospheric record of CO_2 is an important link with $CaCO_3$ processes in the ocean. To a first approximation, atmospheric CO_2 can be considered a proxy for global average surface ocean pCO_2 (Sundquist et al. 1979; Takahashi et al. 1997). This proxy is of great value in estimating past values of surface ocean pCO_2 from estimates of atmospheric CO_2 over geological time. I, therefore, present a digest of what observations and models tell us about the atmospheric CO_2 record over time.

The most detailed contemporary atmospheric CO_2 record available is the temporal variation (published at monthly time steps) in atmospheric CO_2 measured at an elevation of about 3400 m above sea level at an observatory at Mauna Loa, Hawaii (Keeling 1960; Scripps and subsequent NOAA data available at http://www.esrl.noaa.gov/gmd/ccgg/trends/; last accessed 3 Mar 2012). Similar records, albeit for shorter timespans also exist (and can be found on the NOAA Web site) for Barrow, Alaska; American Samoa; the South Pole; Trinidad Head, California; and Summit, Greenland. The annual trends at these sites are in close agreement with one another, whereas seasonal oscillations differ among the sites. Many additional short-term data sets of atmospheric CO_2 can be found in the scientific literature.

Fig. 9a shows the progression of the so-called "Keeling Curve" at Mauna Loa between 1958 and 2012. Over that period, atmospheric CO_2 rose from 315 to 393 parts per million by volume (ppmv). The clear annual oscillation in the signal apparently represents seasonal variation in net primary production (dominated by seasonal variations in Northern Hemisphere terrestrial plant biomass; Pearman and Hyson 1980; Bacastow et al. 1985). The rise is widely attributed to human activities: primarily, the burning of fossil fuels; secondarily, changing patterns of land cover and land use releasing long-term organic C storage back to the atmosphere (e.g., Canadell et al. 2007).

A series of studies (summarized by Lüthi et al. 2008) have extracted CO_2 information from bubbles in ice cores collected in Antarctica (Fig. 9b). This remarkable record starting about 800,000 years before the present (B.P.) and extending forward to about 140 years ago (the Late Quaternary Period) has revealed a pCO_2 oscillation between about 170 and 300 ppmv. The oscillation cycle of approximately 100,000 years represents the glacial–interglacial cycle of atmospheric CO_2 variation. The mechanism (or mechanisms) driving the CO_2 oscillation remains a matter of conjecture and debate (e.g., Sigman and Boyle 2000).

Whereas there are records that are interpreted to represent atmospheric CO_2 further into the geological past, these records are fragmented and not entirely consistent with one another (summarized by Berner 2004a). Models of atmospheric CO_2 have been constructed for the Phanerozoic Eon; two of the more recent and comprehensive CO_2 models over this time scale (~550 million years) have been the GEOCARB III model by Berner and Kothavala (2001) and the model by Bergman et al. (2004). These two models agree remarkably well. An important reminder, as Berner (2004a) observed (p. 99), is that such models are no more than suggestions of how CO_2 has changed over the Phanerozoic. I've chosen to present the Berner and Kothavala (2001) model as Fig. 9c to give a sense of present opinion on long-term variations of atmospheric CO_2.

The two most important points to note about the Phanerozoic models of atmospheric CO_2 are as follows: (1) There is apparently almost a 30-fold variation in pCO_2 according to GEOCARB III (from about 270 to 7300 ppmv), but no obvious cyclicity, at the 10 million year time steps of that model. The lack of obvious cyclicity

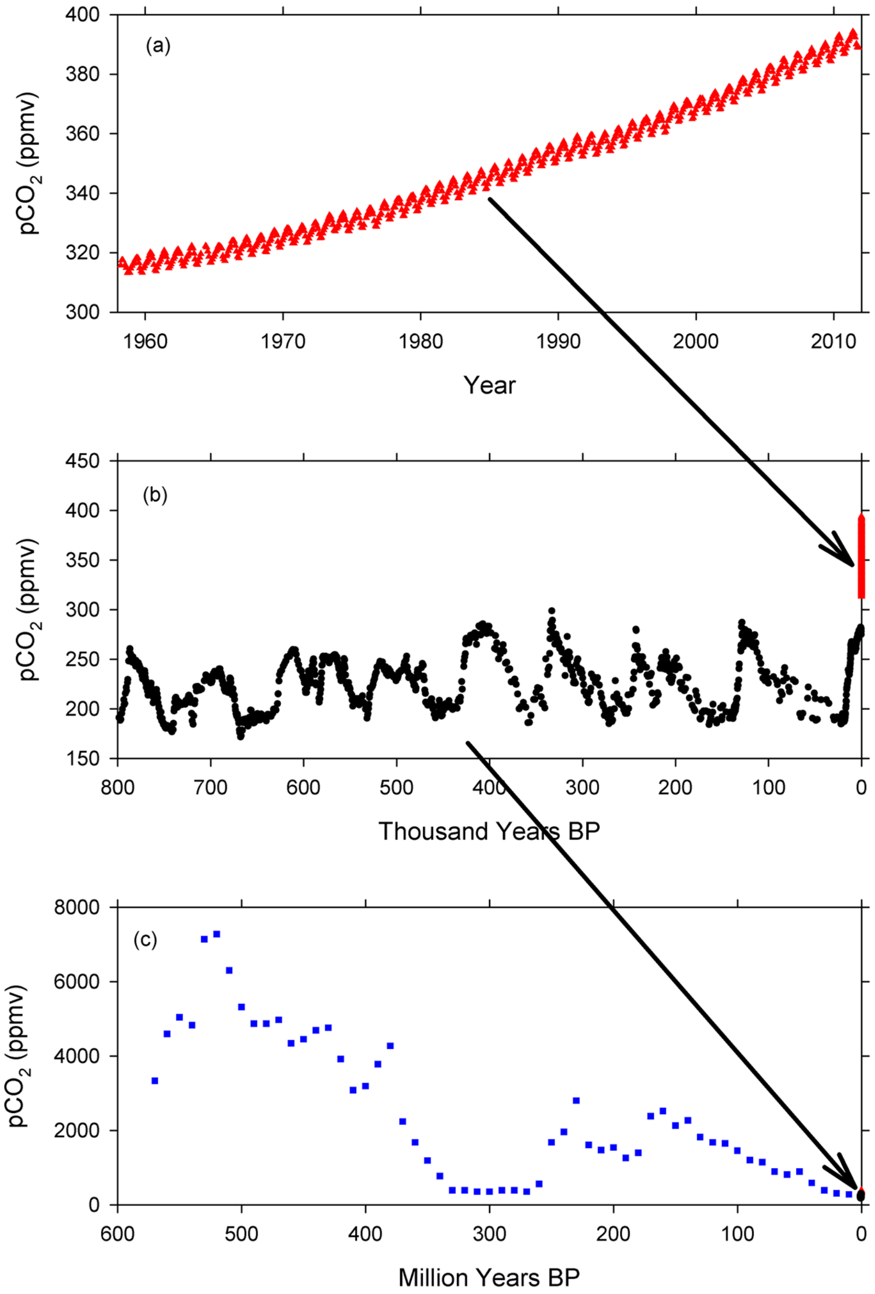

Fig. 9. Variation of atmospheric pCO_2 over three time scales: (a) Variations recorded at Mauna Loa between 1958 and 2012. (b) Variations recorded in air bubbles within ice cores recovered in Antarctica. This record spans approximately the past 800,000 years. (c) Variations modeled by Berner and Kothavala (2001) over the past 570 million years.

is probably not surprising, given the fact that the cyclicity seen in the more finely resolved Late Quaternary data set is about 10^5 years and undetectable in GEOCARB III. (2) Only two intervals in the record (the present, back to about 80 million years B.P.; and ~350-260 million years B.P.) had CO_2 levels below 1000 ppmv. These points will become important in the analysis of $CaCO_3$ reactions over geological time.

Effect of Ψ on CO_2 flux in the post-modern (increasingly acidified) world ocean

I assume that deep ocean values for Ψ change only slowly over time, because of the large mass of TCO_2 and TA in the ocean below 500 m and relatively slow downward mixing of the changing atmospheric signal. By contrast, surface water Ψ (i.e., approximately the mixed layer, ~50-100 m) would be expected to vary rapidly over time as surface-water pCO_2 adjusts to the changing CO_2 content of the overlying atmosphere. Over an atmospheric pCO_2 range of 190 to 500 ppmv (about the range from glacial minimum pCO_2 to twice the pre-industrial interglacial pCO_2), the mean surface Ψ is well-represented by the regression equation

$$\Psi = 1.1 - 6.26 \times pCO_2^{-0.451} \text{ (see \textit{Materials and methods})}.$$

Temperature also affects Ψ (Frankignoulle et al. 1994). This simple regression without temperature is preferred as a generic predictor of global surface ocean Ψ, because of the relative wide range of expected temperature at the Earth surface. At 190 ppmv, average surface Ψ for the low-latitude provinces is estimated to have been about 0.51; at 500 ppmv, the average will be about 0.72 (see also Lerman and Mackenzie 2005).

Fig. 10 is a modification of Fig. 8, to incorporate a surface ocean Ψ of 0.72, the expected value at an atmospheric pCO_2 of 500 ppmv. According to the most recent IPCC projections (http://www.ipcc-data.org/ddc_co2.html; last accessed 2 Mar 2012), this level of atmospheric pCO_2 will be reached by about 2050. The elevated pCO_2 and surface ocean Ψ will result in more CO_2 efflux from surface waters where most $CaCO_3$ production occurs, and no change from deep water dissolution. The net CO_2 efflux associated with benthic production of 30 × 10^{12} mol y^{-1} and deep dissolution of 10 × 10^{12} mol y^{-1} is predicted to be 13 × 10^{12} mol y^{-1}. At this elevated level of pCO_2, flux

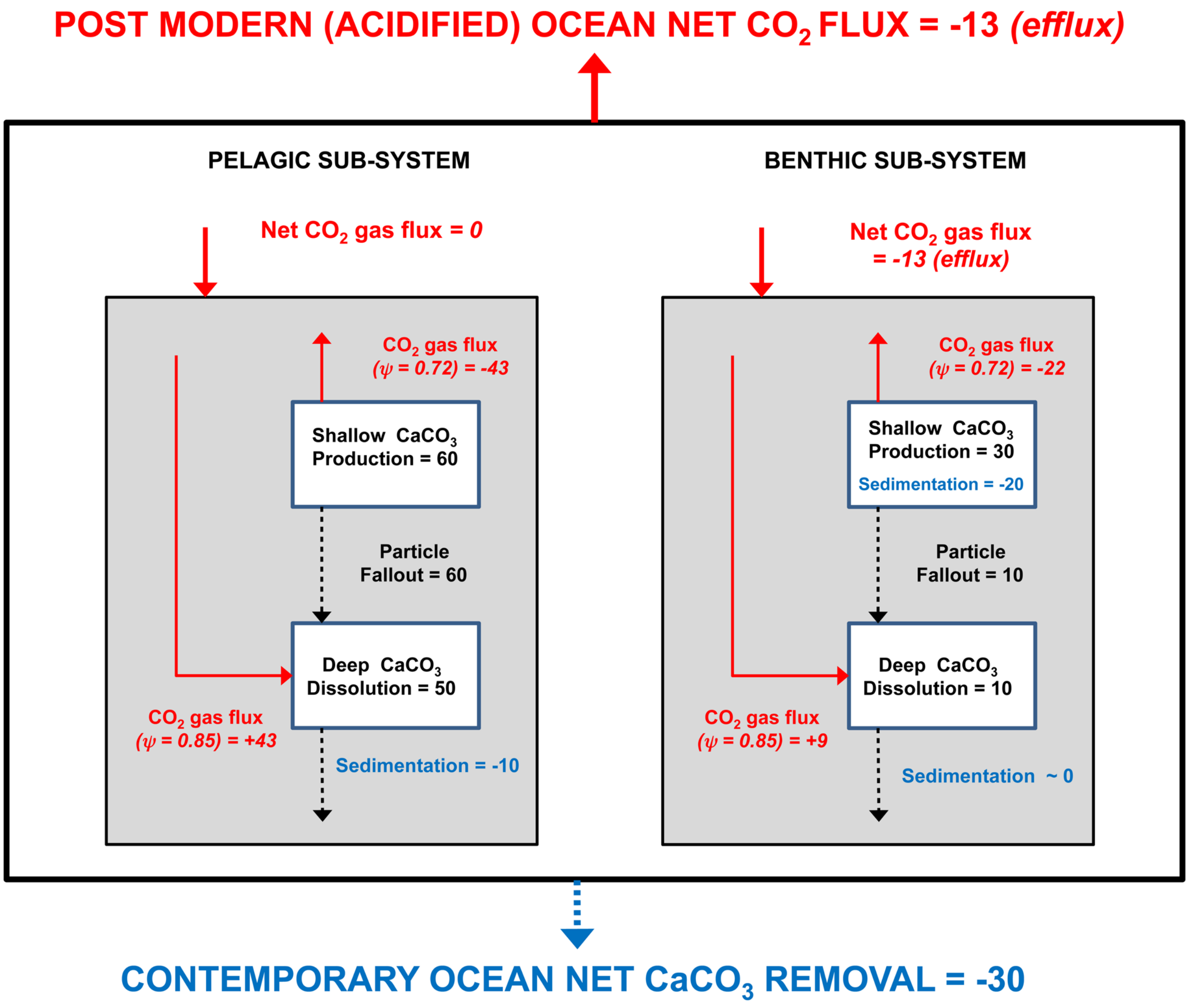

Fig. 10. Post-modern global ocean $CaCO_3$ budget (atmospheric pCO_2 = 500 ppmv; surface ocean Ψ = 0.72), split into pelagic and benthic sub-systems. Fluxes are in units of 10^{12} mol y^{-1}. Note the increase in net CO_2 efflux relative to Fig. 7.

of CO_2 associated with pelagic $CaCO_3$ production minus dissolution will be 0. The total gas efflux from the pelagic + benthic sub-systems predicted for these acidified conditions is about 43% of the prediction from Eq. 1 and 2.6 times the present efflux. The increased efflux will occur as rising atmospheric CO_2 lowers both pH and the bicarbonate buffer capacity of surface seawater. Clearly, net CO_2 flux associated with $CaCO_3$ production, dissolution, and burial is highly sensitive to changes in atmospheric pCO_2 and to surface ocean Ψ.

It should be noted that this simplified model analysis only considers the effect of Ψ. It is very likely (e.g., Smith and Buddemeier 1992; Kleypas et al. 1999; Feely et al. 2004; Orr et al. 2005; Guinotte and Fabry 2008) that changing calcite and aragonite saturation state of surface ocean waters in response to ocean acidification will also affect both benthic and pelagic $CaCO_3$ production rates.

$CaCO_3$-mediated gas flux with glacial-interglacial variations in sea level

A simple simulation puts the gas flux associated with the benthic versus pelagic sub-systems into broader context. The past 120,000 years have taken the planet Earth out of one interglacial period, into and through a glacial period, and then back to the present interglacial.

Fig. 11a (derived from Fig. 9b) shows changes in atmospheric CO_2: from about 270 ppmv during the last interglacial (120,000 years B.P.), falling to about 190 by the Last Glacial Maximum (LGM, 20,000 B.P.), and then rising rapidly to 280 during the present interglacial. CO_2 emissions over about the past 140 years have further boosted atmospheric pCO_2 to the contemporary level of about 390 ppmv; also shown.

Fig. 11b shows calculated Ψ as a function of pCO_2. Over the pCO_2 range of ~190 to 280 ppmv of the last glacial cycle, surface ocean Ψ is estimated to have varied between 0.51 and 0.61. Recent CO_2 emissions have further elevated Ψ to 0.63. Based on Frankignoulle et al. (1994), Lerman and Mackenzie (2005), Smith and Gattuso (2011), and Waelbroeck et al. (2009), I estimate that a temperature change of <3°C between the present and the LGM would cause an increase in Ψ of < 0.02. This temperature effect is ignored here.

Sea level is also shown during this cycle (Fig. 11c) (from about 20 m above present sea level 120,000 B.P. to about 120 m below present sea level during the LGM, 20,000 B.P.; then back to the present sea level; Miller et al. 2005).

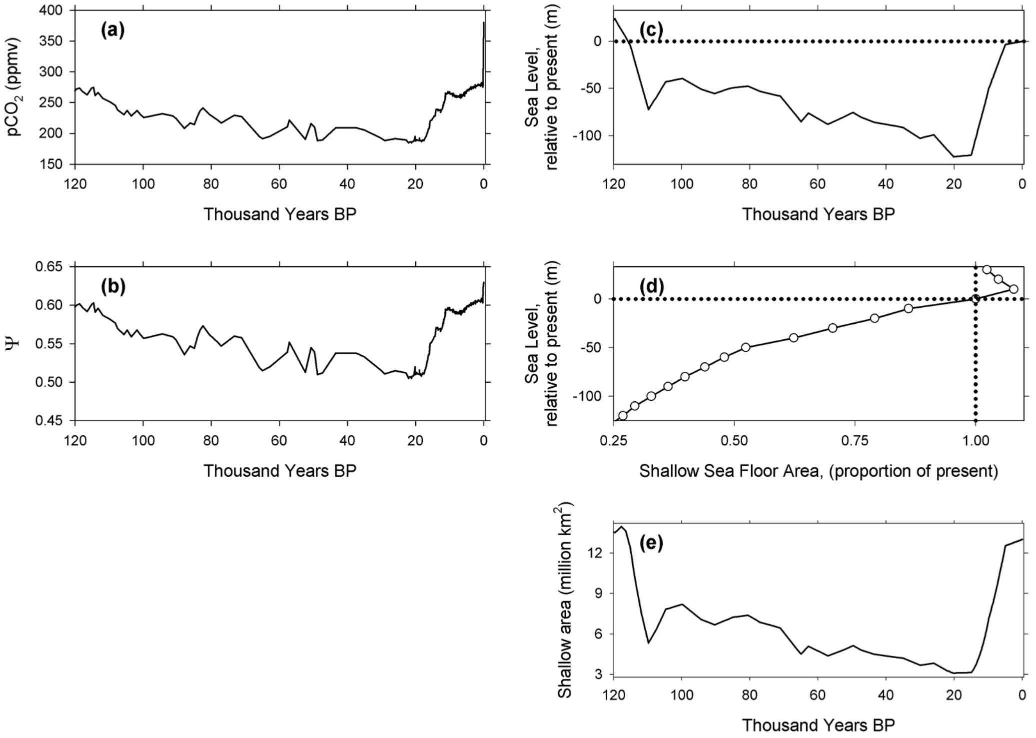

Fig. 11. (a) Variation in atmospheric pCO_2 over the past 120,000 years (the most recent interglacial—glacial cycle). (b) Average surface ocean Ψ for the low-latitude ocean provinces as a function of atmospheric CO_2 ($\Psi = 0.39 + 0.00063 \times pCO_2$) over the past 120,000 years. (c) Sea level (relative to present) over the past 120,000 years. (d) Sea floor area shallower than 50 m (as a proportion of the present) over the range of relative sea levels in Fig. 9c. (e) Estimated sea floor area shallower than 50 m (km^2) over the past 120,000 years.

Changing benthic $CaCO_3$ production is simulated as follows. It is assumed that benthic production primarily occurs on sea floor that lies within 50 m of the sea surface, and that this production is proportional to total oceanic shallow benthic area. The present hypsographic curve of global elevation between –170 m and +30 m is used to calculate changing "shallow sea floor area" within 50 m of the sea surface as a function of sea level changes from the present (Fig. 11d). $CaCO_3$ production per unit area is assumed to have remained constant.

Fig. 11e presents the estimated area of sea floor shallower than 50 m over the past glacial cycle. That area has varied from about 13.4 × 10^6 km^2 (slightly greater than the estimated present area of 13 × 10^6 km^2) at the peak of the last interglacial period to a minimum of about 3.3 × 10^6 km^2 near the LGM—a 4-fold variation in shallow benthic area available for benthic $CaCO_3$ production, with the interglacial periods being the times of maximum available area.

Benthic $CaCO_3$ production, dissolution, accumulation, and net CO_2 gas flux are scaled relative to the estimates of contemporary fluxes (Table 3; Fig. 8). $CaCO_3$ production and dissolution associated with the pelagic sub-system are assumed to have remained constant, whereas net gas flux from pelagic reactions varied according the pCO_2 dependence estimated from surface ocean Ψ (Fig. 10b) with a constant deep-water Ψ value of 0.85.

Fig. 12a describes the variation of $CaCO_3$ production as a result of changing benthic $CaCO_3$ production while pelagic production and dissolution are assumed to have remained constant. Pelagic $CaCO_3$ production has remained substantially higher than benthic production over the 120,000 years represented by the diagram. Accumulation provides a different situation (Fig. 12b). Except for the period from about 65,000 B.P. and leading into the last glacial maximum (LGM, ~ 20,000 B.P.), benthic $CaCO_3$ accumulation has apparently approximately equaled or substantially exceeded pelagic accumulation.

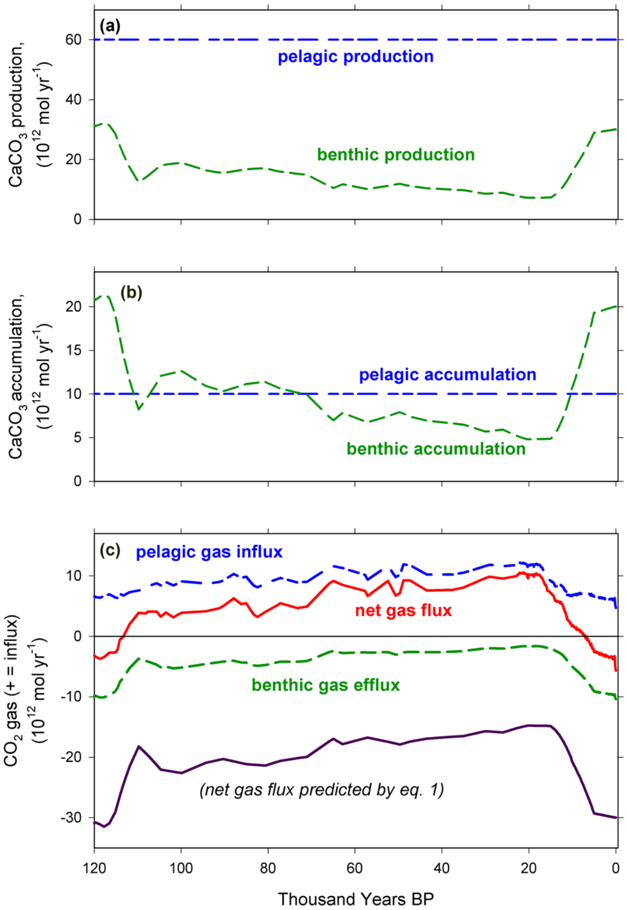

Fig. 12. (a) Benthic $CaCO_3$ production over the past 120,000 years, based on assumptions in text; pelagic production is assumed to remain constant. (b) Benthic $CaCO_3$ accumulation, based on assumptions in text. (c). Benthic, pelagic, and total CO_2 gas fluxes. The surface flux applies the pCO_2-dependent value for Ψ as a function of atmospheric pCO_2, whereas the deep dissolution, accumulation, and gas fluxes are assumed to remain constant proportions of the surface production fluxes. This figure also includes the fluxes which would be predicted from the "standard equation" (Eq. 1) for CO_2 gas flux in response to $CaCO_3$ accumulation.

The latter part of the present interglacial period (~ the past 7,000 years) has been an interval of low net CO_2 efflux, spiking to 5 × 10^{12} mol y^{-1} in response to anthropogenic rises in CO_2 over the past century (Fig. 11c). During intervals when sea level was more than about 60 m below the present (i.e., ~65,000 to 11,000 B.P.), the CO_2 flux would have been dominated by CO_2 influx associated with the planktonic sub-system. At the time of the LGM, net $CaCO_3$-associated CO_2 gas influx would have represented an oceanic CO_2 sink of about 11 × 10^{12} mol y^{-1}.

For comparison, Fig. 12c also shows the net gas flux that is estimated for the global ocean according to Eq. 1 over the past interglacial–glacial cycle. Not only is the Eq. 1 flux greatly different than the estimated flux using variable surface ocean Ψ, but also the flux is, of course, always negative (gas efflux). This poses a striking contrast between Eq. 1 as an estimator of $CaCO_3$-induced CO_2 gas flux and the model results presented here.

The simple "relative habitat area" estimate of changing benthic $CaCO_3$ production may somewhat underestimate the diminution of benthic production during glaciation. Waelbroeck et al. (2009) estimated that the global tropical and subtropical ocean was about 1.7°C cooler than the present during the LGM, whereas the tropical/subtropical Atlantic was almost 3°C cooler. The budgetary estimates of Milliman and Droxler (1996) indicate that about 2/3 of benthic

$CaCO_3$ production is by coral reefs and other shallow-water tropical communities, so the cooler LGM temperatures may have narrowed the geographic range of these communities. It seems likely, however, that calcifying communities or individual organisms more tolerant of cooler, temperate waters could have, at least, partially compensated for a temperature-related shift (Chave 1968; Milliman and Droxler 1996).

Other shifts associated with diminished input of fresh water, sediments, and nutrients during the glacial interval have probably also impacted the $CaCO_3$ budget. Such effects, while potentially important, are outside the purview of the present analysis.

I have simulated the effects of Ψ only for the most recent glacial–interglacial cycle. One can assume similar effects during the glacial–interglacial oscillations of the past million years (Sigman and Boyle 2000; Lüthi et al. 2008), throughout the rest of the Quaternary Period (to ~3 million years B.P.; http://www.geosociety.org/science/timescale/; last accessed 4 June 2012), and perhaps back as far as 23 million years B.P. (the Neogene Period; Fig. 9c). It seems likely, from an extension of Fig. 12, that this period dominated by glaciation has also been dominated by $CaCO_3$-mediated CO_2 influx into the ocean, except for the relatively brief interglacial periods.

Variation of Ψ over Phanerozoic time

Atmospheric pCO_2 has apparently been below about 500 ppmv for approximately the past 20-30 million years (Fig. 9c; also see Pagani et al. 2005). For this interval of geological time, I assume that $CaCO_3$-associated CO_2 flux in the ocean has generally followed the contemporary (interglacial) and glacial flux patterns as laid out in the previous sections. Previous to this time interval, atmospheric pCO_2 was much higher—apparently up to about 7000 ppmv for most of the previous 550 million years. The only early interval with atmospheric CO_2 below 1000 ppmv was during the late Paleozoic, between about 350 and 260 million years B.P. (Fig. 9c).

Ψ is calculated over the course of Phanerozoic time according to the regression equation given in *Materials and methods* (Fig. 13). Also included in the figure is evidence presented by Hardie (1996) of variations in composition of the Phanerozoic oceans. The mineralogy of nonskeletal marine carbonate mineralogy has varied between being dominantly aragonite + high Mg calcite and dominantly low Mg calcite. The variation in carbonate mineralogy may represent an effect of $CaCO_3$ saturation state, with the more soluble aragonite + high Mg calcite minerals representing periods of higher saturation state. The aragonitic periods appear to be intervals during which seawater composition was richer in $MgSO_4$, whereas the calcitic intervals appear to have been richer in KCl. These variations in seawater ion ratios and $CaCO_3$ saturation state were probably characterized by varying carbonic acid dissociation constants, representing a complicating factor in the calculation of Ψ from the contemporary dissociation constants.

Further, I have not attempted to include the effect of temperature on Ψ, so the model calculations are no more than a semiquantitative example of how this coefficient would have varied over deep geological time. Nor have I attempted to estimate the relative rates of benthic versus pelagic $CaCO_3$ production and accumulation,

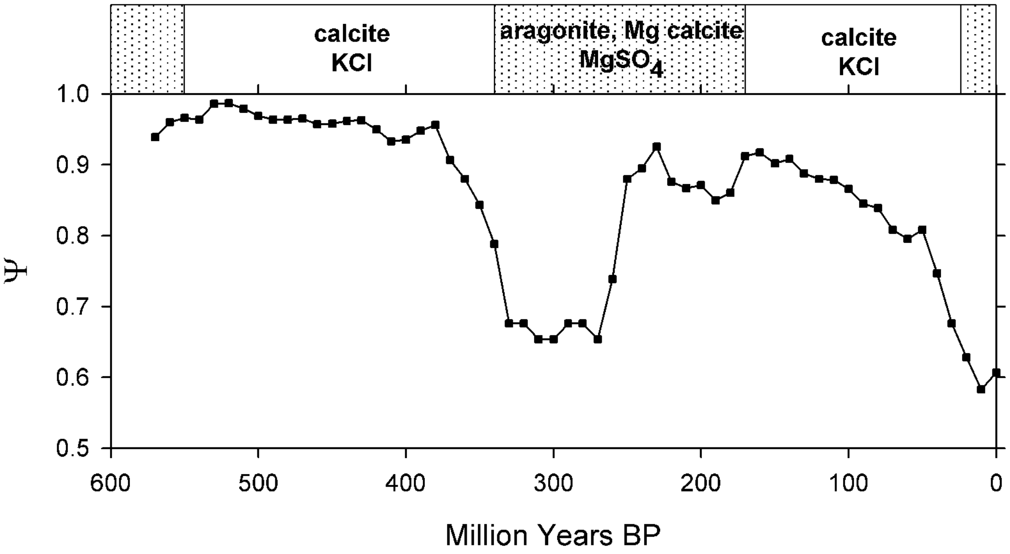

Fig. 13. Variation of Ψ over Phanerozoic time.

because sea floor spreading, sediment discharge to the shelf areas, and major variations of ocean area and volume make any reconstruction of shallow ocean area extremely speculative.

Employing the Berner and Kothavala (2001) GEOCARB III model estimates of atmospheric pCO_2 over Phanerozoic time, the only two intervals with Ψ significantly below 1.0 appear to have been about the past 70 million years (i.e., the Quaternary through the Paleogene Periods) and the interval between 350 and 260 million years B.P. (Carboniferous and Permian Periods). The Carboniferous–Permian low pCO_2 interval, like the current interval, appears to have been a period with extensive glaciation analogous to the past 3 million years (Royer et al. 2004).

During these intervals of low Ψ, relationships analogous to those developed for the past 800,000 to 3 million years would have probably applied. That is, the difference between benthic $CaCO_3$ production and dissolution would have acted as a source of CO_2 release to the atmosphere; the difference between pelagic production and dissolution would have acted as an atmospheric CO_2 sink.

The remainder of Phanerozoic time, with high pCO_2, would have seen a very different response to $CaCO_3$ production and dissolution. Temperature and alkalinity effects on Ψ would have been small, and Ψ would have approached 1.0 (i.e., as predicted by Eq. 1). Differences between surface ocean and deep ocean Ψ would have been small. The feedback between oceanic $CaCO_3$ accumulation and CO_2 release to the atmosphere would have been close to unity and largely insensitive to pelagic versus benthic subsystems of $CaCO_3$ production, dissolution, and accumulation.

As atmospheric CO_2 dropped over the past 70 million years, from about 1000 ppmv, surface ocean Ψ and the difference between surface and deep ocean Ψ would have approached the range of values we now observe. The adjustments in Ψ would have been more rapid for surface waters than for deep water because of the relatively small mass of dissolved inorganic C in surface waters and the intimate exchange of CO_2 gas across the air-sea interface.

In this context, see the analysis by Kiessling (2006) suggesting that the early Phanerozoic period between about 400 and 350 million years B.P. was the period of dominant reef volume in the geologic record. Copper (1994) derived much the same conclusion and extended the conclusion to include all benthic carbonate deposition.

This drop is unlikely to have been related in any direct way to $CaCO_3$ reactions. For at least two reasons, this period of dominating contribution of reefs and other benthic sites to $CaCO_3$ deposition would have experienced net CO_2 efflux from the ocean to the atmosphere. First, by analogy with the present, most benthic production accumulated, rather than dissolving lower in the water column. Second, the high pCO_2 of this interval would have led to Ψ values approaching 1.0 (Fig. 13), with little variation through the water column.

By contrast with these periods of domination by benthic $CaCO_3$ production, the interval between 350 and 260 million years B.P. was probably analogous with the Quaternary history of CO_2 flux oscillating between low net CO_2 efflux and influx. This pattern has apparently prevailed at least over the past 20 million years and very likely as much as 50 million years or somewhat more (Fig. 13).

These observations about atmospheric CO_2 concentrations, Ψ, $CaCO_3$ accumulation, and sea-air CO_2 flux over Phanerozoic time are very general, in order to illustrate the potential secular variability of these variables and the importance of such variability. I have based the calculation of Ψ in the surface ocean strictly on atmospheric CO_2, with the implicit assumption that seawater composition has remained constant. Yet it is by now well-established that there have been substantial secular variations in the major ion composition of seawater (particularly Ca, Mg, K, SO_4; Fig. 13). This variation has been recognized and described based on data summarized by various authors (e.g., Hardie 1996; Horita et al. 2002; Lowenstein et al. 2003) and appears to be relatively well represented in two detailed global geochemical models (Berner 2004a; Arvidson et al. 2006).

It becomes an issue of interest for long-term reconstruction of $CaCO_3$-mediated sea-air gas exchange, to establish more precisely how both surface and deep water Ψ and benthic versus pelagic $CaCO_3$ production and accumulation shifted over this timespan.

Chapter 5. Discussion

The analysis presented here generally confirms, for the contemporary global ocean, results which Smith and Gattuso (2011) reported for the Central Pacific Ocean. The vertical variation of the coefficient Ψ, the molar ratio between CO_2 air-sea gas flux and $CaCO_3$ reactions in the world ocean, plays a significant role in the ocean–atmosphere carbon balance. As a result, the net CO_2 efflux from the contemporary oceanic gross versus net $CaCO_3$ production is much lower than predicted by Eq. 1, and the net flux has been CO_2 invasion into the ocean during significant portions of the past 3 million to 20+ million years. For most of geological history previous to 70 million years B.P., pCO_2 was substantially higher; Ψ was near 1.0, probably with little vertical variation of Ψ. Equation 1 is at least an approximate indicator of $CaCO_3$-mediated CO_2 flux during this time span. The sole major exception for which evidence of low pCO_2 exists is between about 350 and 260 million years B.P.

An explanation for the sensitivity of atmospheric CO_2 to proportionally large variations when pCO_2 is low becomes evident when the $CaCO_3$ production and dissolution components are explicitly separated into benthic versus pelagic components. $CaCO_3$ production by the pelagic sub-system of the contemporary open ocean dominates gross $CaCO_3$ flux, but most of that material dissolves in the water column rather than accumulating. Because of the vertical variation of Ψ relative to the loci of $CaCO_3$ production and dissolution, the difference between pelagic $CaCO_3$ production and dissolution creates a net CO_2 sink—not a source, even though there is some accumulation of $CaCO_3$. By contrast, most $CaCO_3$ produced by the benthic sub-system escapes dissolution (or dissolves in situ, at the same effective Ψ as the material was produced). As a result, there is net CO_2 efflux associated with net $CaCO_3$ accumulation in the benthic sub-system.

When the pelagic and benthic sub-systems are combined for the contemporary global ocean, net $CaCO_3$ accumulation is a slight net CO_2 source. The present strength of this source ($\sim 5 \times 10^{12}$ mol y^{-1}) is far weaker than would have been anticipated from a direct application of Eq. 1 to the net $CaCO_3$ accumulation of $\sim 30 \times 10^{12}$ mol y^{-1}. The anticipated CO_2 efflux would have been 30×10^{12}—not 5×10^{12}—mol y^{-1}.

Both forecasting Ψ to be expected from higher atmospheric CO_2 over the next few decades and hindcasting over the past glacial cycle demonstrate the sensitivity of the net gas flux:carbonate precipitation ratio to atmospheric CO_2, and to changing proportions of benthic and planktonic $CaCO_3$ accumulation (Figs. 8-11). Rising atmospheric pCO_2 and surface ocean Ψ are pushing the oceanic $CaCO_3$ cycle toward increased net CO_2 flux into the atmosphere, whereas lowered surface Ψ and lowered shallow benthic seafloor area for benthic $CaCO_3$ production during periods of glaciation led to substantial CO_2 absorption.

A large $CaCO_3$-induced CO_2 sink during glacial sea level low stands would have been sufficient to exhaust atmospheric CO_2 rapidly (on a time scale of the order of 10^4 years). This is unrealistic, so there must be compensating and causally linked CO_2 sources to offset that sink. Evidence can be found for one possible link in widespread erosion of exposed shelf sedimentary deposits during the low stands, accompanied by oxidation of sedimentary organic matter deposited in these shallow waters (e.g., Talling 1998; Gensous and Tesson 1996; Hanebuth et al. 2003; Fullthorpe and Austin 2004). This would have released CO_2 to the atmosphere, at least partially offsetting the CO_2 sink from pelagic domination of $CaCO_3$ production and dissolution.

The analysis presented here is a new variation on the idea (apparently originating with Milliman 1974; explicitly formulated as "the coral reef hypothesis" by Berger 1982; explored in further detail by Opdyke and Walker 1992 and Vecsei and Berger 2004) of the possible role of benthic versus planktonic $CaCO_3$ production, dissolution, preservation, and net CO_2 gas flux during the glacial-interglacial cycle in controlling atmospheric CO_2.

The important point that has previously escaped attention is the role played by the difference between the vertical distribution of $CaCO_3$ production and dissolution, within the context of vertically variable Ψ and differing contributions of pelagic and benthic production and dissolution to net fluxes. The benthic sub-cycle is always a CO_2 source. The pelagic sub-cycle is a CO_2 sink, as long as the vertical difference in Ψ is sufficiently large for dissolution-mediated uptake of CO_2 to offset precipitation-mediated release. This combined effect occurs even though both sub-cycles are net producers of $CaCO_3$. The total cycle switches between being a source or sink, depending on the relative contributions of the two sub-cycles to the total cycle and on the vertical variation of Ψ. Vertically variable Ψ, along with variable benthic versus pelagic net $CaCO_3$ accumulation, is clearly not the only control on atmospheric CO_2 variations over time, but it should not be ignored.

A tenet in the analysis of the long-term (rock) cycle of carbon is that atmospheric CO_2 consumed by weathering of limestone on land should balance CO_2 release to the atmosphere during the formation of $CaCO_3$ (e.g., Berner 2004b). The contemporary net CO_2 efflux estimated in Fig. 8 (5×10^{12} mol y^{-1}) differs, but not greatly, from the uptake of CO_2 by weathering in areas dominated by carbonate rocks (~9×10^{12} mol y^{-1}) as estimated by Amiotte Suchet et al. (2003). The oceanic CO_2 efflux is associated with a contemporary net $CaCO_3$ production of 30×10^{12} mol y^{-1}, while the CO_2 influx is associated with about 17×10^{12} mol y^{-1} of weathering in areas dominated by carbonate rocks (Amiotte Suchet et al. 2003).

These flux differences between estimates of carbonate rock weathering on land and oceanic $CaCO_3$ accumulation, while relatively small for totally independent budgetary estimates, might arise from non–steady state behavior of the rock contributions to the global C cycle. CO_2 flux variation over the past interglacial–glacial cycle has been ~10×10^{12} mol y^{-1} (Fig. 11c), leading to non–steady state, oscillating variations in atmospheric CO_2.

A point of further, relevant interest is raised in a recent paper by Liu et al. (2011). Those authors argued that CO_2 uptake by limestone weathering on land may also be influenced by $\Psi < 1.0$. As those authors recognize, the matter remains to be resolved.

Chapter 6. Summary and Conclusions

Equation 1 is a qualitatively useful—but quantitatively inaccurate—description of $CaCO_3$ precipitation and dissolution in the contemporary ocean. Evidence leading toward this conclusion has been accumulating since the early 1940s. The present analysis expands understanding of the significance to be drawn from this conclusion.

The molar ratio of CO_2 efflux to $CaCO_3$ precipitation, in that part of the contemporary (surface) ocean where $CaCO_3$ production primarily occurs, averages about 0.63, whereas the gas absorption:dissolution ratio in deeper waters is ~0.85. The gas flux:$CaCO_3$ reaction ratio, termed Ψ, of the surface ocean changes over time as surface water pCO_2 equilibrates with the changing overlying atmospheric composition. Ψ of deeper waters undoubtedly fluctuates as well, but the large mass of dissolved inorganic C in deep water must limit the speed of this deep water fluctuation. The observations that the ratio Ψ is < 1.0, variable through the oceanic water column, and variable over time lead to some heretofore unrecognized conclusions about the oceanic $CaCO_3$ cycle.

The thematic question behind the present analysis can be framed as follows: Is the oceanic $CaCO_3$ cycle, including $CaCO_3$ precipitation, dissolution, and accumulation, a net atmospheric CO_2 source, or a sink? The answer to this question is, necessarily, nuanced.

The oceanic $CaCO_3$-mediated CO_2 pump is an oscillating pump that reverses between being an atmospheric CO_2 source and a sink. The magnitude and oscillation of the pump depend upon (1) temporal variations in the absolute and relative rates of planktonic and benthic $CaCO_3$ production and dissolution; (2) temporal variations in atmospheric pCO_2; and (3) vertical and temporal variations in pCO_2 and Ψ in the oceanic water column.

Present, near-future, and past time scale reconstructions of apparent characteristics of this pump demonstrate that the pump can be expected to respond to anthropogenically generated changes in atmospheric CO_2 over the next few decades, just as it has responded to long-term variations in shallow sea floor areas and atmospheric CO_2 over geological time.

The oceanic $CaCO_3$ cycle is, of course, only one sub-cycle of the various parts of the global C cycle. C flux through this sub-cycle is relatively slow compared with organic C fluxes (the other major biogeochemical sub-cycle of C), but the total C stored in limestone (primarily marine-derived limestone) exceeds C storage in all other components of the atmosphere, hydrosphere, biosphere, and the Earth's crust (Sigman and Boyle 2000). Therefore this relatively slowly cycling—but cumulatively large—reservoir of C must be evaluated carefully in the overall global C cycle.

References

Amiotte Suchet, P., J.-L. Probst, and W. Ludwig. 2003. Worldwide distribution of continental rock lithology: implications for the atmospheric/soil CO_2 uptake by continental weathering and alkalinity river transport to the oceans. Global Biogeochem. Cycles 17:1038 [doi:10.1029/2002GB001891].

Arvidson, R. S., F. T. Mackenzie, and M. Guidry. 2006. MAGic: a Phanerozoic model for the geochemical cycling of major rock-forming components. Am. J. Sci. 306:135-190 [doi:10.2475/ajs.306.3.135].

Bacastow, R. B., C. D. Keeling, and T. P. Whorf. 1985. Seasonal amplitude increase in atmospheric CO_2 concentration at Mauna Loa, Hawaii, 1959-1982. J. Geophys. Res. 90:10529-10540 [doi:10.1029/JD090iD06p10529].

Barker, S., J. A. Higgins, and H. Elderfield. 2003. The future of the carbon cycle: review, calcification response, ballast and feedback on atmospheric CO_2. Phil. Trans. R. Soc. Lond. A 361:1977-1999 [doi:10.1098/rsta.2003.1238].

Berger, W. H. 1982. Increase of carbon dioxide in the atmosphere during deglaciation: the coral reef hypothesis. Naturwissenschaften 69:87-88 [doi:10.1007/BF00441228].

Bergman, N. M., T. M. Lenton, and A. J. Watson. 2004. COPSE: a new model of biogeochemical cycling over Phanerozoic time. Am. J. Sci. 304:397-437 [doi:10.2475/ajs.304.5.397].

Berner, R. A. 2004a. The Phanerozoic carbon cycle: CO_2 and O_2. Oxford Univ. Press.

———. 2004b. A model for calcium, magnesium and sulfate in seawater over Phanerozoic time. Am. J. Sci. 304:438-453 [doi:10.2475/ajs.304.5.438].

———, and Z. Kothavala. 2001. GEOCARB III: revised model of atmospheric CO_2 over Phanerozoic time. Am. J. Sci. 301:182-204 [doi:10.2475/ajs.301.2.182].

Broecker, W. S., and T. Takahashi. 1966. Calcium carbonate precipitation on the Bahama Banks. J. Geophys. Res. 71:1575-1602 [doi:10.1029/JZ071i006p01575].

Burdige, D. J. 2005. Burial of terrestrial organic matter in marine sediments: a re-assessment. Global Biogeochem. Cycles 19:GB4011 [doi:10.1029/2004GB002368].

Canadell, J. G., and others. 2007. Contributions to accelerating atmospheric CO_2 growth from economic activity, carbon intensity, and efficiency of natural sinks. Proc. Nat. Acad. Sci. USA 104:18866-18870 [doi:10.1073/pnas.0702737104].

Catubig, N. R., D. E. Archer, R. Francois, P. deMenocal, W. Howard, and E.-F. Yu. 1998. Global deep-sea burial rate of calcium carbonate during the last glacial maximum. Paleoceanography 13:298-310 [doi:10.1029/98PA00609].

Chave, K. E. 1968. Recent carbonate sediments—an unconventional view. J. Geol. Educ. 15:200-204.

Copper, P. 1994. Ancient reef ecosystem expansion and collapse. Coral Reefs 13:3-11 [doi:10.1007/BF00426428].

Crutzen, P. J. 2002. Geology of mankind. Nature 415:23 [doi:10.1038/415023a].

Darwin, C. 1842. The structure and distribution of coral reefs. Being the first part of the geology of the voyage of the Beagle, under the command of Capt. Fitzroy, R. N., during the years 1832 to 1836. Mith Elder and Co.

D'Elia, C. F., and A. R. Harris. 2008. The R/V Alpha Helix Expedition: a retrospective analysis of a milestone in coral reef research, Vol. 1:38-42 (Session number 1), *In* Proc. 11th International Coral Reef Symposium, Ft. Lauderdale, FL. ReefBase: A Global Information System on Coral Reefs [Online]. Available from: <http://www.nova.edu/ncri/11icrs/proceedings/files/m01-09.pdf> [Accessed: February 5, 2013].

Dickson, A. G., C. L. Sabine, and J. R. Christian [eds.]. 2007. Guide to best practices for ocean CO_2 measurements. PICES Special Pub. 3. <http://www.pices.int/publications/special_publications/default.aspx>.

Drew, G. H. 1913. On the precipitation of calcium carbonate in the sea by marine bacteria, and on the action of denitrifying bacteria in tropical and temperate seas. J. Mar. Biol. Assoc. U. K. 9:479-524 [doi:10.1017/S0025315400071526].

Egleston, E. S., C. L. Sabine, and F. M. M. Morel. 2010. Revelle revisited: buffer factors that quantify the response of ocean chemistry to changes in DIC and alkalinity. Global Biogeochem. Cycles 24 [doi:10.1029/2008GB003407].

England, M. H. 1995. The age of water and ventilation timescales in a global ocean model. J. Phys. Ocean 25:2756-2777 [doi:10.1175/1520-0485(1995)025<2756:TAOWAV>2.0.CO;2].

Feely, R. A., C. L. Sabine, K. Lee, W. Berelson, J. Kleypas, V. J. Fabry, and F. J. Millero. 2004. Impact of anthropogenic CO_2 on the $CaCO_3$ system in the oceans. Science 305:362-366 [doi:10.1126/science.1097329].

Frankignoulle, M., C. Canon, and J.-P. Gattuso. 1994. Marine calcification as a source of carbon dioxide: positive feedback of increasing atmospheric CO_2. Limnol. Oceanogr. 39:458-462 [doi:10.4319/lo.1994.39.2.0458].

Fullthorpe, C. S., and J. A. Austin, Jr. 2004. Shallowly buried, enigmatic seismic stratigraphy on the New Jersey outer shelf: evidence for latest Pleistocene catastrophic erosion? Geology 32:1013-1016 [doi:10.1130/G20822.1].

Gattuso, J.-P., and L. Hansson. 2011. Ocean acidification. Oxford Univ. Press.

Gensous, B., and M. Tesson. 1996. Sequence stratigraphy, seismic profiles, and cores of Pleistocene deposits on the Rhône continental shelf. Sed. Geol. 105:183-190 [doi:10.1016/0037-0738(95)00135-2].

Guinotte, J. M., and V. J. Fabry. 2008. Ocean acidification and its potential effects on marine ecosystems. Ann. N. Y. Acad. Sci. 1134:320-342 [doi:10.1196/annals.1439.013].

Hanebuth, T. J. J., K. Stattegger, A. Schimanski, T. Lüdmann, and H. K. Wong. 2003. Late Pleistocene forced-regressive deposits on the Sunda Shelf (Southeast Asia). Mar. Geol. 199:139-157 [doi:10.1016/S0025-3227(03)00129-4].

Hardie, L. A. 1996. Secular variation in seawater chemistry: An explanation for the coupled secular variation in the mineralogies of marine limestones and potash evaporites over the past 600 m.y. Geology 24:279-283 [doi:10.1130/0091-7613(1996)024<0279:SVISCA>2.3.CO;2].

Hedges, J. I., and R. G.Keil. 1995. Sedimentary organic matter preservation: an assessment and speculative synthesis. Mar. Chem. 49:81-115 [doi:10.1016/0304-4203(95)00008-F].

Horita, J., H. Zimmermann, and H. D. Holland. 2002. Chemical evolution of seawater during the Phanerozoic: implications from the record of marine evaporites. Geochim. Cosmochim. Acta 66: 3733-3756.

Iglesias-Rodriguez, M. D., and others. 2002. Progress made in study of ocean's calcium carbonate budget. EOS 83:365-375 [doi:10.1029/2002EO000267].

Johannes, R. E., and others. 1972. Metabolism of some coral reef communities: a team study of nutrient and energy flux at Eniwetok. BioScience 22:541-543 [doi:10.2307/1296314].

Johnson, K. M., and others. 1998. Coulometric total carbon dioxide analysis for marine studies: assessment of the quality of total inorganic carbon measurements made during the US Indian Ocean CO_2 Survey 1994-1996. Mar. Chem. 63:21-37 [doi:10.1016/S0304-4203(98)00048-6].

Kawahata, H., A. Suzuki, and K. Goto. 1997. Coral reef ecosystems as a source of atmospheric CO_2: evidence from pCO_2 measurements of surface waters. Coral Reefs 16:261-266 [doi:10.1007/s003380050082].

Keeling, C. D. 1960. The concentration and isotopic abundances of carbon dioxide in the atmosphere. Tellus 12:200-203 [doi:10.1111/j.2153-3490.1960.tb01300.x].

Kennedy, W. J., and R. E. Garrison. 1975. Morphology and genesis of nodular chalks and hardgrounds in the Upper Cretaceous of southern England. Sedimentology 22:311-386 [doi:10.1111/j.1365-3091.1975.tb01637.x].

Kiessling, W. 2006. Towards an unbiased estimate of fluctuations in reef abundance and volume during the Phanerozoic. Biogeosciences 3:15-27 [doi:10.5194/bg-3-15-2006].

Kinsey, D. W. 1972. Preliminary observations on community metabolism and primary productivity of the pseudo-atoll reef at One Tree Island, Great Barrier Reef. Proc. Symp., p. 13-32. *In* Corals and coral reefs. Mar. Biol. Assoc. India.

Kleypas, J. A., R. W. Buddemeier, D. Archer, J.-P. Gattuso, C. Langdon, and B. N. Opdyke. 1999. Geochemical consequences of increased atmospheric carbon dioxide on coral reefs. Science 284:118-120 [doi:10.1126/science.284.5411.118].

Kohn, A. J., and P. Helfrich. 1957. Organic productivity of a Hawaiian coral reef. Limnol. Oceanogr. 2:241-251.

Ladd, H. S., and S. O. Schlanger. 1960. Drilling operations on Eniwetok Atoll, p. 863-903 *In* U. S. Geol. Surv. Prof. Paper 260-Y.

———, J. I. Tracey, Jr., and M. G. Gross. 1967. Drilling on Midway Atoll, Hawaii. Science 156:1098-1094 [doi:10.1126/science.156.3778.1088].

Laws, E. A., P. G. Falkowski, W. O. Smith, Jr., H. Ducklow, and J. J. McCarthy. 2000. Temperature effects on export production in the open ocean. Global Biogeochem. Cycles 14:1231-1246 [doi:10.1029/1999GB001229].

Lee, K. 2001. Global net community production estimated from the annual cycle of surface water total dissolved inorganic carbon. Limnol. Oceanogr. 46:1287-1297 [doi:10.4319/lo.2001.46.6.1287].

Lerman, A., and F. T. Mackenzie. 2005. CO_2 air-sea exchange due to calcium carbonate and organic matter storage, and its implications for the global carbon cycle. Aquat. Geochem. 11:345-390 [doi:10.1007/s10498-005-8620-x].

Lewis, E., and D. W. R. Wallace. 1998. Program developed for CO_2 system calculations. ORNL/CDIAC-105, Carbon Dioxide Information Analysis Center, Oak Ridge National Laboratory, U. S. Department of Energy. <http://cdiac.esd.ornl.gov/oceans/co2rprt.html>.

Lowenstein, T. K., L. A. Hardie, M. N. Timofeeff, and R. V. Demicco. 2003. Secular variation in seawater chemistry and the origin of calcium chloride basinal brines. Geology 31:857-860 [doi:10.1130/G19728R.1].

Li, Y.-H., T. Takahashi, and W. S. Broecker. 1969. Degree of saturation of $CaCO_3$ in the oceans. J. Geophys. Res. 74:5507-5525 [doi:10.1029/JC074i023p05507].

Liu, Z., W. Dreybrodt, and H. Liu. 2011. Atmospheric CO_2 sink: silicate weathering or carbonate weathering? Appl. Geochem. 26: S292-S294 [doi:10.1016/j.apgeochem.2011.03.085].

Lüthi, D., and others. 2008. High-resolution carbon dioxide concentration record 650,000-800,000 years before present. Nature 453:379-382 [doi:10.1038/nature06949].

Mackenzie, F. T., A. Andersson, A. Lerman, and L. M. Ver. 2005. Boundary exchanges in the global coastal margin: implications for the organic and inorganic carbon cycles. Chapter 7, p. 193-225. *In* A. R. Robinson and K. H. Brink [eds.], The global coastal ocean: Multiscale interdisciplinary processes, The sea, v. 13. Harvard Univ. Press.

Martin, W. R., and F. L. Sayles. 1996. $CaCO_3$ dissolution in sediments of the Ceara Rise, western equatorial Atlantic. Geochim. Cosmochim. Acta 60:243-263 [doi:10.1016/0016-7037(95)00383-5].

Miller, K. G., and others. 2005. The Phanerozoic record of global sea-level change. Science 310:1293-1298 [doi:10.1126/science.1116412].

Millero, F. J., and others. 1998. Assessment of the quality of the shipboard measurements of total alkalinity on the WOCE Hydrographic Program Indian Ocean CO_2 survey cruises 1994-1996. Mar. Chem. 63:9-20 [doi:10.1016/S0304-4203(98)00043-7].

Milliman, J. D. 1974. Marine carbonates. Springer.

———. 1993. Production and accumulation of calcium carbonate in the ocean: a budget of a nonsteady state. Global Biogeochem. Cycles 7:927-957 [doi:10.1029/93GB02524].

———, and A. W. Droxler. 1996. Neritic and pelagic carbonate sedimentation in the marine environment: ignorance is not bliss. Geologische Rundschau 85:496-504 [doi:10.1007/BF02369004].

———, P. J. Troy, W. M. Balch, A. K. Adams, Y.-H. Li, and F. T. Mackenzie. 1999. Biologically mediated dissolution of calcium carbonate above the chemical lysocline? Deep Sea Res. I 46:1653-1669 [doi:10.1016/S0967-0637(99)00034-5].

Morse, J. W., and F. T. Mackenzie. 1990. Geochemistry of sedimentary carbonates. Elsevier.

Murray, J., and A. F. Renard. 1891. Report on deep-sea deposits based on the specimens collected during the voyage of H. M. S. *Challenger* in the years 1872 to 1876. Challenger Reports.

Odum, H. T., and E. P. Odum. 1955. Trophic structure and productivity of a windward coral reef community on Eniwetok Atoll. Ecol. Monogr. 25:291-320 [doi:10.2307/1943285].

Opdyke, B. N., and J. C. G. Walker. 1992. Return of the coral reef hypothesis: basin to shelf partitioning of $CaCO_3$ and its effect on atmospheric CO_2. Geology 20:733-736 [doi:10.1130/0091-7613(1992)020<0733:ROTCRH>2.3.CO;2].

Orr, J. C., and others. 2005. Anthropogenic ocean acidification over the twenty-first century and its impact on calcifying organisms. Nature 437 [doi:10.1038/nature04095].

Pagani, M., J. C. Zachs, K. H. Freeman, B. Tipple, and S. Bohaty. 2005. Marked decline in atmospheric carbon dioxide concentrations during the Paleogene. Science 309:600-603 [doi:10.1126/science.1110063].

Pearman, G. I., and P. Hyson. 1980. Activities in the global biosphere as reflected in atmospheric CO_2 records. J. Geophys. Res. 85:4468-4474 [doi:10.1029/JC085iC08p04457].

Raven, J. A., and P. G. Falkowski. 1999. Oceanic sinks for atmospheric CO_2. Plant Cell Environ. 22:741-755 [doi:10.1046/j.1365-3040.1999.00419.x].

Revelle, R., and H. E. Suess. 1957. Carbon dioxide exchange between the atmosphere and ocean and the question of an increase of atmospheric CO_2 during the past decades. Tellus 9:18-27 [doi:10.1111/j.2153-3490.1957.tb01849.x].

Royer, D. L., R. A. Berner, I. P. Montañez, N. J. Tabor, and D. J. Beerling. 2004. CO_2 as a primary driver of Phanerozoic climate. GSA Today 14:4-10 [doi:10.1130/1052-5173(2004)014<4:CAAPDO>2.0.CO;2].

Sargent, M. C., and T. S. Austin. 1954. Biologic economy of coral reefs. Bikini and nearby atolls, Part 2, Oceanography (biologic). U. S. Geol. Surv. Prof. Paper 260-E: 293-300.

Sigman, D. M., and E. A. Boyle. 2000. Glacial/interglacial variations in atmospheric carbon dioxide. Nature 407:859-868 [doi:10.1038/35038000].

Smith, C. L. 1940a. The Great Bahama Bank, 1, General hydrographical and chemical features. J. Mar. Res.3:147-170.

———. 1940b. The Great Bahama Bank, 2, Calcium carbonate precipitation. J. Mar. Res.3:171-189.

Smith, S. V. 1973. Carbon dioxide dynamics: a record of organic carbon production, respiration, and calcification in the Eniwetok windward reef flat community. Limnol. Oceanogr.18:106-120 [doi:10.4319/lo.1973.18.1.0106].

———. 1984. Phosphorus versus nitrogen limitation in the marine environment. Limnol. Oceanogr. 29:1149-1160 [doi:10.4319/lo.1984.29.6.1149].

———. 1985. Physical, chemical and biological characteristics of CO_2 gas flux across the air-water interface. Plant Cell Environ. 8:387:398 [doi:10.1111/j.1365-3040.1985.tb01674.x].

———, and F. Pesret. 1974. Processes of carbon dioxide flux in the Fanning Atoll Lagoon. Pac. Sci. 28:225-245.

———, and P. L. Jokiel. 1978. Water composition and biogeochemical gradients in the Canton Atoll lagoon. Atoll Res. Bull. 221:16-53.

———, and M. J. Atkinson. 1984. Phosphorus limitation of net production in a confined aquatic ecosystem. Nature 307:626-627 [doi:10.1038/307626a0].

———, and H. H. Veeh. 1989. Mass balance of biogeochemically active materials (C, N, P) in a hypersaline gulf. Est. Coast. Shelf Sci. 29:195-215 [doi:10.1016/0272-7714(89)90053-X].

———, and R. W. Buddemeier. 1992. Global change and coral reef ecosystems. Ann. Rev. Ecol. Syst. 23:89-118 [doi:10.1146/annurev.es.23.110192.000513].

———, and J. -P. Gattuso. 2011. Balancing the oceanic calcium carbonate cycle: consequences of variable water column Ψ. Aquat. Geochem. 17:327-337 [doi:10.1007/s10498-010-9109-9].

Sundquist, E. T. 1993. The global carbon dioxide budget. Science 259:934-941.

———, L. N. Plummer, and T. M. L. Wigley. 1979. Carbon dioxide in the ocean surface: the homogeneous buffer factor. Science 204:1203-1205 [doi:10.1126/science.204.4398.1203].

Sverdrup, H. U., M. W. Johnson, and R. H. Fleming. 1942. The Oceans. Their physics, chemistry and general biology. Prentice-Hall.

Takahashi, T., R. A. Feely, R. F. Weiss, R. H. Wanninkhof, D. W. Chipman, S. C. Sutherland, and T. T. Takahashi. 1997. Global air-sea flux of CO_2: an estimate based on measurements of sea-air pCO_2 difference. Proc. Nat. Acad. Sci. USA 94:8292-8299 <http://www.pnas.org/content/94/16/8292.full>.

Talling, P. J. 1998. How and where do incised valleys form if sea level remains above the shelf edge? Geology 26:87-90 [doi:10.1130/0091-7613(1998)026<0087:HAWDIV>2.3.CO;2].

Vecsei, A., and W. H. Berger. 2004. Increase of atmospheric CO_2 during deglaciation: constraints on the coral reef hypothesis from patterns of deposition. Global Biogeochem. Cycles 18 [doi:10.1029/2003GB002147].

Waelbroeck, C., and others. 2009. Constraints on the magnitude and patterns of ocean cooling at the Last Glacial Maximum. Nat. Geosci. 2:127-132 [doi:10.1038/ngeo411].

Ware, J. R., S. V. Smith, and M. L. Reaka-Kudla. 1991. Coral reefs: sources or sinks of atmospheric CO_2? Coral Reefs 11:127-130 [doi:10.1007/BF00255465].

Wollast, R. 1994. The relative importance of biomineralization and dissolution of $CaCO_3$ in the global carbon cycle. Bull. Inst. Oceanogr. 13:13-35.

———, R. M. Garrels, and F. T. Mackenzie. 1980. Calcite-seawater reactions in ocean surface waters. Am. J. Sci. 280:831-848 [doi:10.2475/ajs.280.9.831].

Appendix 1

Table A1. Data variables in summary tables. Data bin-averaged as described in text.

1	Depth (m)
2	Temperature (C)
3	Salinity (psu)
4	Sigma-t
5	PO_4 (µmol kg^{-1})
6	SiO_4 (µmol kg^{-1})
7	TCO_2^* (µmol kg^{-1}, normalized to a salinity of 35)
8	TA* (µeq kg^{-1}, normalized to a salinity of 35)
9	TA*(n) (µeq kg^{-1}, normalized to a salinity of 35 and corrected for nutrient contribution)
10	pCO_2 (µatm, calculated from TCO_2 and TA)
11	Ω_c (calcite saturation state; calculated as described in text)
12	Ψ (CO_2 gas:$CaCO_3$ reaction ratio; calculated as described in text)

Appendix 2

Table A2. Gulf of Alaska

Depth	Temp.	Salinity	sigma_t	PO_4	SiO_4	TCO_2*	TA*	TA*(n)	pCO_2	Ω_c	Ψ
19.1	7.751	32.6803	25.5252	1.17	21.14	1898.2	2057.3	2045.1	351.1	2.976	0.760
72.7	4.031	32.8917	26.4182	1.62	32.04	1967.5	2080.8	2067.0	434.9	2.229	0.812
121.5	3.751	33.3189	27.0201	2.09	49.10	2064.2	2133.1	2115.5	672.1	1.653	0.857
172.0	3.865	33.6339	27.5057	2.46	64.93	2138.8	2174.2	2158.2	920.4	1.287	0.887
214.7	4.030	33.7769	27.8069	2.60	72.43	2173.6	2192.5	2179.4	1056.1	1.117	0.900
274.7	3.639	33.8179	28.1643	2.72	80.36	2193.0	2204.1	2193.1	1098.1	1.022	0.907
313.9	3.787	33.9186	28.4178	2.86	89.28	2221.3	2218.8	2209.5	1232.5	0.906	0.916
378.3	3.284	33.9025	28.7571	2.86	91.74	2221.1	2224.0	2215.4	1148.0	0.919	0.914
408.6	3.806	34.0433	28.9619	2.99	100.48	2251.7	2240.4	2232.5	1322.8	0.825	0.922
475.4	3.705	34.1018	29.3330	3.01	109.18	2266.7	2261.6	2254.6	1252.0	0.849	0.920
508.5	3.637	34.1289	29.5162	3.04	109.43	2271.2	2255.6	2248.3	1362.3	0.779	0.925
591.5	2.845	34.0719	29.9417	2.97	117.12	2259.3	2264.5	2257.0	1112.5	0.892	0.914
608.4	3.450	34.2034	30.0631	3.09	119.21	2287.4	2270.2	2263.1	1373.2	0.754	0.926
687.4	3.288	34.2590	30.4936	3.08	127.05	2297.7	2294.5	2288.1	1219.0	0.824	0.919
709.3	3.318	34.2678	30.5999	3.11	126.36	2301.4	2293.6	2287.1	1268.3	0.792	0.921
790.0	2.770	34.2343	31.0092	3.05	136.68	2293.1	2294.4	2287.7	1151.4	0.829	0.917
808.4	3.104	34.3107	31.1203	3.12	133.03	2308.6	2295.0	2288.0	1324.2	0.744	0.924
887.7	2.921	34.3461	31.5380	3.07	139.90	2314.6	2319.0	2312.3	1138.8	0.840	0.915
908.5	2.952	34.3566	31.6404	3.13	138.38	2318.9	2302.0	2290.3	1404.2	0.747	0.923
985.5	2.610	34.3435	32.0267	3.06	150.15	2313.4	2318.1	2311.7	1118.0	0.818	0.915
1123.7	2.613	34.4148	32.7263	3.11	150.99	2327.2	2323.3	2316.4	1206.6	0.746	0.920
1370.8	2.355	34.4833	33.9576	3.09	159.49	2335.9	2341.9	2335.5	1102.3	0.759	0.914
1599.0	2.154	34.5268	35.0724	3.05	165.42	2334.7	2345.7	2338.7	1053.4	0.749	0.911
1862.9	1.974	34.5670	36.3430	2.98	165.71	2327.5	2356.1	2348.3	909.7	0.807	0.900
2108.4	1.843	34.6000	37.5152	2.92	169.31	2326.0	2357.7	2350.8	873.2	0.776	0.898
2378.3	1.732	34.6236	38.7843	2.84	169.31	2314.5	2362.3	2355.7	757.6	0.819	0.887
2591.6	1.668	34.6366	39.7769	2.80	168.72	2309.8	2357.5	2350.0	758.5	0.782	0.887
2867.4	1.612	34.6487	41.0462	2.73	165.66	2296.2	2361.0	2353.9	653.8	0.828	0.874
3085.6	1.566	34.6586	42.0497	2.71	168.15	2294.7	2357.5	2350.0	662.9	0.776	0.876
3370.5	1.539	34.6650	43.3418	2.63	163.96	2280.0	2356.0	2347.5	596.5	0.800	0.865
3565.7	1.507	34.6735	44.2313	2.63	165.72	2281.9	2352.9	2344.6	617.0	0.739	0.870
3876.6	1.485	34.6791	45.6276	2.56	160.43	2267.8	2353.1	2345.1	546.1	0.760	0.858
4061.4	1.488	34.6827	46.4529	2.52	154.18	2268.3	2352.8	2346.2	542.9	0.724	0.859
4384.5	1.502	34.6864	47.8860	2.48	157.75	2259.6	2354.0	2347.2	501.9	0.720	0.851
4591.8	1.531	34.6854	48.7913	2.50	155.58	2262.9	2350.2	2343.5	528.8	0.657	0.858
4870.6	1.549	34.6881	50.0142	2.47	156.33	2256.0	2347.7	2341.2	508.1	0.637	0.854
5104.1	1.560	34.6887	51.0356	2.45	152.56	2247.4	2338.8	2331.2	510.1	0.605	0.854
5355.6	1.580	34.6879	52.1244	2.44	152.96	2247.0	2340.3	2334.0	497.3	0.580	0.853
5659.2	1.610	34.6883	53.4343	2.43	146.22	2237.4	2321.7	2314.5	531.4	0.511	0.861

Appendix 3

Table A3. North Pacific Ocean.

Depth	Temp.	Salinity	sigma_t	PO$_4$	SiO$_4$	TCO$_2$*	TA*	TA*(n)	pCO$_2$	Ω_c	Ψ
22.8	23.542	34.4927	23.3822	0.20	2.56	1947.1	2244.5	2237.7	365.7	5.131	0.632
77.4	20.568	34.6828	23.5841	0.38	4.36	1995.3	2268.1	2272.0	400.4	4.635	0.660
125.0	18.002	34.7636	25.5432	0.57	7.09	2035.8	2274.4	2247.5	448.9	4.058	0.694
177.8	15.151	34.6422	26.3781	0.86	11.36	2061.1	2258.1	2231.4	501.7	3.392	0.734
226.2	13.951	34.5569	26.8016	0.91	13.11	2061.5	2247.6	2223.6	498.0	3.197	0.744
279.4	12.322	34.4559	27.3140	1.19	18.48	2081.2	2237.1	2211.6	567.1	2.748	0.773
324.1	11.253	34.3697	27.6669	1.32	21.26	2086.3	2227.3	2204.5	586.3	2.514	0.788
384.5	9.973	34.3374	28.1525	1.66	29.86	2118.5	2231.5	2209.6	680.6	2.129	0.816
416.4	9.327	34.2995	28.3699	1.73	33.56	2120.4	2227.9	2206.9	684.0	2.041	0.821
486.0	8.272	34.2649	28.8553	2.05	43.35	2150.7	2233.2	2216.0	777.8	1.709	0.846
514.6	7.684	34.2009	29.0275	2.06	46.87	2147.2	2224.1	2207.6	784.4	1.632	0.851
589.7	6.691	34.2700	29.5889	2.50	60.81	2198.2	2247.1	2234.5	934.3	1.309	0.877
615.8	6.079	34.2024	29.7452	2.51	65.19	2195.2	2240.1	2228.1	932.8	1.254	0.881
688.9	5.727	34.2948	30.2091	2.72	74.78	2226.9	2262.1	2252.1	993.0	1.142	0.889
719.7	5.202	34.2415	30.3840	2.79	81.21	2233.9	2257.7	2248.4	1062.3	1.033	0.898
787.3	4.937	34.3341	30.8037	2.87	88.15	2251.3	2278.4	2269.6	1026.7	1.040	0.897
814.9	4.503	34.2715	30.9387	2.89	94.00	2252.2	2268.8	2260.4	1092.6	0.948	0.905
887.8	4.524	34.3924	31.3685	2.94	98.20	2268.4	2292.6	2284.4	1034.7	0.991	0.900
916.9	4.157	34.3575	31.5249	3.04	107.60	2281.9	2293.2	2286.0	1126.1	0.886	0.909
988.0	4.060	34.4231	31.9155	2.99	107.92	2280.6	2305.5	2296.2	1022.4	0.979	0.899
1112.5	3.581	34.4512	32.5741	3.02	119.93	2295.5	2315.7	2307.6	1036.1	0.910	0.903
1383.8	2.919	34.5177	33.9619	3.00	136.54	2310.1	2336.5	2328.8	959.7	0.893	0.900
1621.5	2.483	34.5628	35.1477	2.94	146.22	2313.6	2348.3	2340.5	882.5	0.898	0.895
1898.4	2.167	34.6034	36.4918	2.84	151.24	2310.1	2358.9	2351.3	774.8	0.931	0.885
2142.5	1.936	34.6229	37.6558	2.77	154.21	2306.3	2361.3	2353.9	726.0	0.918	0.881
2399.0	1.790	34.6432	38.8625	2.72	156.08	2299.7	2363.9	2356.5	668.1	0.923	0.874
2613.0	1.697	34.6499	39.8545	2.67	155.05	2294.2	2363.5	2356.3	635.7	0.909	0.870
2898.8	1.610	34.6635	41.1725	2.61	154.49	2286.8	2362.9	2356.0	595.8	0.892	0.865
3125.8	1.565	34.6670	42.2069	2.58	153.45	2280.9	2359.6	2352.5	580.7	0.861	0.863
3405.6	1.523	34.6760	43.4779	2.54	152.56	2274.6	2358.2	2351.3	554.6	0.835	0.859
3621.4	1.497	34.6810	44.4522	2.50	150.46	2268.7	2355.2	2347.9	541.0	0.812	0.857
3906.1	1.473	34.6840	45.7280	2.48	149.27	2262.1	2353.0	2346.4	517.0	0.783	0.854
4128.8	1.473	34.6868	46.7212	2.46	146.89	2256.7	2345.3	2338.1	525.1	0.734	0.856
4418.3	1.476	34.6894	48.0001	2.43	145.46	2252.2	2344.7	2338.0	505.8	0.707	0.853
4615.6	1.477	34.6908	48.8712	2.42	143.03	2246.3	2337.9	2331.0	507.0	0.672	0.853
4890.8	1.474	34.6931	50.0809	2.39	140.18	2239.0	2334.9	2327.9	488.3	0.652	0.850
5114.5	1.492	34.6939	51.0544	2.38	138.52	2235.0	2328.7	2321.3	495.6	0.612	0.852
5377.9	1.520	34.6938	52.1956	2.37	137.44	2230.9	2326.0	2318.8	487.9	0.584	0.851
5719.9	1.561	34.6949	53.6655	2.37	135.47	2225.5	2319.6	2312.2	489.8	0.540	0.852

Appendix 4

Table A4. South Pacific Ocean.

Depth	Temp.	Salinity	sigma_t	PO$_4$	SiO$_4$	TCO$_2$*	TA*	TA*(n)	pCO$_2$	Ω_c	Ψ
22.0	23.942	35.2951	23.8990	0.33	1.58	2036.4	2348.5	2342.4	387.3	5.246	0.631
77.9	21.780	35.3228	24.7468	0.45	2.30	2058.4	2349.0	2338.6	400.6	4.840	0.652
127.6	19.092	35.3644	25.7237	0.66	3.73	2097.9	2352.2	2333.2	449.4	4.223	0.687
180.2	16.148	35.2099	26.5932	0.95	6.56	2122.3	2330.8	2306.8	515.4	3.511	0.729
229.7	14.666	35.0835	27.0643	1.06	7.06	2125.2	2312.9	2288.4	542.1	3.184	0.748
283.8	12.801	34.9036	27.5834	1.34	10.29	2135.7	2290.0	2265.8	609.1	2.698	0.779
326.8	11.907	34.8339	27.9135	1.46	11.87	2140.5	2283.0	2261.6	620.9	2.510	0.790
387.2	9.623	34.6222	28.4619	1.77	14.96	2146.6	2258.7	2239.9	677.0	2.082	0.819
423.4	9.444	34.6458	28.6862	1.77	16.71	2150.1	2262.9	2247.7	653.3	2.061	0.819
488.1	7.803	34.5062	29.1463	1.98	18.96	2149.3	2249.4	2232.1	673.1	1.878	0.831
518.5	7.666	34.5057	29.3105	1.93	20.28	2146.0	2250.3	2236.3	632.9	1.902	0.828
589.5	6.699	34.4483	29.7377	2.12	24.58	2154.1	2246.6	2230.5	672.8	1.741	0.839
620.5	6.642	34.4629	29.9007	2.12	27.99	2157.6	2251.9	2239.0	648.5	1.738	0.838
689.5	5.971	34.4181	30.2792	2.22	29.98	2159.0	2246.0	2228.8	685.8	1.645	0.844
721.6	5.932	34.4296	30.4419	2.16	32.39	2157.6	2252.0	2240.7	619.9	1.691	0.839
788.8	5.428	34.4212	30.8141	2.32	38.31	2170.6	2255.3	2242.6	662.7	1.567	0.848
822.4	5.380	34.4378	30.9885	2.29	42.43	2172.1	2260.1	2250.3	631.5	1.579	0.846
887.3	4.854	34.4192	31.3447	2.41	45.94	2181.1	2260.3	2249.2	668.4	1.469	0.854
919.3	4.863	34.4354	31.5031	2.35	48.69	2180.0	2263.5	2255.5	632.5	1.490	0.851
987.3	4.406	34.4464	31.8860	2.50	56.98	2197.0	2272.7	2263.9	666.7	1.392	0.858
1132.3	3.900	34.4766	32.6444	2.50	67.51	2207.9	2283.6	2275.4	652.1	1.343	0.859
1377.4	3.152	34.5443	33.9227	2.58	89.19	2236.4	2306.6	2296.4	677.3	1.227	0.865
1620.2	2.664	34.5908	35.1390	2.56	103.00	2248.6	2324.4	2317.9	620.8	1.192	0.862
1883.3	2.312	34.6249	36.4192	2.53	112.89	2255.7	2335.6	2329.2	593.2	1.152	0.859
2146.4	2.077	34.6471	37.6712	2.50	120.66	2259.3	2343.9	2337.5	566.2	1.119	0.856
2387.2	1.935	34.6613	38.8004	2.47	123.05	2257.9	2343.4	2335.2	564.5	1.068	0.855
2618.5	1.835	34.6691	39.8716	2.46	126.64	2258.8	2346.9	2340.7	542.0	1.027	0.854
2874.6	1.758	34.6768	41.0497	2.43	126.64	2254.4	2344.7	2338.8	527.6	0.982	0.852
3137.0	1.683	34.6829	42.2485	2.41	127.81	2250.8	2343.0	2337.0	516.1	0.936	0.851
3386.0	1.629	34.6885	43.3797	2.37	127.18	2245.4	2340.5	2334.3	501.9	0.903	0.849
3630.6	1.562	34.6928	44.4875	2.35	126.68	2239.4	2335.3	2329.0	495.0	0.858	0.848
3880.2	1.472	34.6972	45.6182	2.32	126.05	2231.9	2329.4	2323.1	483.4	0.818	0.847
4132.8	1.385	34.7007	46.7566	2.29	123.13	2221.5	2320.7	2314.8	470.3	0.779	0.846
4395.1	1.294	34.7029	47.9339	2.25	121.20	2211.8	2312.7	2306.8	458.5	0.742	0.844
4636.3	1.220	34.7057	49.0123	2.23	119.53	2203.0	2303.6	2297.9	453.7	0.700	0.844
4880.2	1.153	34.7074	50.0955	2.20	118.86	2195.3	2298.3	2292.6	441.3	0.673	0.842
5121.2	1.148	34.7084	51.1535	2.19	118.20	2191.2	2292.7	2287.1	443.7	0.632	0.844
5386.0	1.197	34.7076	52.2948	2.19	119.19	2191.0	2292.4	2286.7	444.0	0.598	0.844
5624.6	1.218	34.7074	53.3226	2.19	119.09	2188.0	2290.1	2284.4	440.2	0.571	0.844

Appendix 5

Table A5. Arctic Ocean.

Depth	Temp.	Salinity	sigma_t	PO_4	SiO_4	TCO_2*	TA*	TA*(n)	pCO_2	Ω_c	Ψ
16.3	7.440	34.8829	27.2930	0.57	3.23	2073.4	2269.4	2262.4	332.3	3.339	0.739
77.6	6.170	34.9618	27.8154	0.79	5.71	2099.8	2267.0	2262.1	370.7	2.862	0.768
127.7	6.118	35.0050	28.0889	0.86	6.53	2114.6	2279.9	2276.1	375.7	2.803	0.771
183.3	6.383	35.0299	28.3402	0.88	6.93	2113.8	2276.8	2273.8	383.1	2.734	0.773
225.8	5.676	35.0293	28.6175	0.92	7.14	2122.3	2278.7	2273.0	393.8	2.626	0.780
289.9	5.807	35.0135	28.9020	0.94	7.65	2114.8	2267.9	2264.7	395.3	2.535	0.783
323.5	5.603	34.9939	29.0696	0.95	7.92	2127.8	2289.4	2285.7	377.2	2.638	0.776
384.6	4.993	34.9835	29.4153	0.97	8.07	2115.7	2264.6	2259.9	393.7	2.428	0.787
424.2	6.106	35.0439	29.5117	0.95	8.00	2129.3	2289.1	2286.8	386.9	2.554	0.778
487.7	4.915	34.9837	29.9072	0.99	8.42	2117.6	2265.2	2261.7	392.2	2.353	0.789
522.9	5.126	34.9690	30.0419	1.01	8.52	2127.9	2282.1	2279.3	381.7	2.425	0.783
588.1	4.356	34.9659	30.4324	1.02	9.04	2114.8	2258.5	2253.2	394.2	2.252	0.793
626.6	5.218	34.9897	30.5260	1.02	8.88	2130.6	2281.8	2279.4	389.4	2.333	0.786
683.4	4.296	34.9482	30.8760	1.03	9.17	2118.1	2261.7	2258.5	388.6	2.201	0.793
727.6	4.974	35.0018	31.0290	1.05	9.20	2135.3	2278.5	2270.9	417.7	2.201	0.794
785.1	3.770	34.9376	31.4034	1.06	9.72	2110.9	2251.4	2247.3	386.0	2.107	0.796
831.3	4.106	34.9227	31.5754	1.06	9.40	2128.8	2274.0	2271.1	382.5	2.151	0.793
884.0	4.121	34.9391	31.8317	1.04	9.78	2114.9	2257.0	2254.0	386.4	2.082	0.795
931.3	4.612	34.9664	32.0104	1.10	10.31	2136.8	2280.8	2278.5	394.7	2.095	0.794
986.2	3.104	34.9324	32.4121	1.06	10.03	2106.8	2245.2	2239.4	381.0	1.985	0.798
1137.8	3.498	34.9089	33.0684	1.06	10.21	2116.6	2254.8	2251.4	384.2	1.923	0.799
1380.8	2.994	34.8919	34.2424	1.05	10.32	2107.1	2246.8	2243.4	368.0	1.828	0.798
1619.4	3.031	34.8809	35.3344	1.04	10.33	2102.9	2245.1	2241.8	360.0	1.757	0.796
1878.0	2.676	34.8863	36.5708	1.03	10.61	2097.9	2238.1	2234.2	357.3	1.635	0.798
2140.4	2.707	34.8994	37.7797	1.03	10.95	2102.0	2243.1	2239.1	355.8	1.552	0.798
2383.3	2.638	34.9139	38.9071	1.02	11.69	2099.2	2241.1	2237.6	350.2	1.474	0.798
2630.9	2.442	34.9139	40.0615	1.02	12.09	2101.9	2241.0	2236.4	354.9	1.374	0.801
2876.6	2.181	34.9087	41.2099	0.99	12.00	2097.2	2238.6	2232.8	345.9	1.317	0.799
3126.8	1.978	34.8986	42.3638	0.99	11.62	2099.3	2237.3	2233.2	345.6	1.218	0.803
3370.1	1.851	34.8923	43.4755	0.98	11.04	2100.9	2241.2	2237.9	335.8	1.169	0.801
3545.4	1.075	34.8862	44.3840	0.98	10.70	2095.2	2236.4	2229.8	326.6	1.122	0.801

Appendix 6

Table A6. North Atlantic Ocean.

Depth	Temp.	Salinity	sigma_t	PO_4	SiO_4	TCO_2*	TA*	TA*(n)	pCO_2	Ω_c	Ψ
18.3	20.214	35.7149	25.0708	0.14	1.50	2074.8	2387.6	2384.2	343.7	5.132	0.637
76.4	17.704	35.9693	26.1964	0.34	2.40	2132.2	2412.4	2405.2	377.5	4.525	0.671
127.2	16.075	36.0428	26.9520	0.52	3.48	2166.2	2418.8	2410.8	409.1	4.053	0.697
181.9	13.929	35.7861	27.5190	0.73	5.00	2167.6	2385.8	2376.8	436.5	3.530	0.727
228.8	13.882	35.8299	27.7848	0.71	4.94	2168.8	2390.9	2381.6	429.0	3.549	0.724
286.3	12.707	35.6372	28.1492	0.91	6.73	2169.6	2368.0	2355.7	462.8	3.197	0.745
326.4	12.667	35.6735	28.3767	0.86	6.15	2171.6	2372.1	2359.8	458.1	3.197	0.743
389.7	10.770	35.3810	28.8039	1.15	9.19	2167.5	2336.2	2322.3	499.3	2.743	0.771
429.7	11.733	35.5482	28.9463	1.01	7.64	2172.6	2355.7	2344.3	477.7	2.905	0.758
491.1	10.299	35.3345	29.3206	1.23	10.40	2169.0	2332.2	2320.4	498.0	2.616	0.776
526.5	9.859	35.3000	29.5548	1.25	10.39	2165.9	2324.9	2314.7	494.2	2.535	0.779
589.7	8.743	35.1504	29.9165	1.41	13.15	2169.1	2311.1	2300.5	521.2	2.293	0.795
626.7	9.014	35.2147	30.0873	1.38	12.61	2172.9	2318.7	2310.5	509.7	2.319	0.792
686.6	8.561	35.1960	30.4322	1.37	12.95	2168.8	2313.2	2306.2	498.3	2.263	0.794
733.2	8.315	35.1739	30.6738	1.40	13.54	2170.8	2312.1	2306.3	498.7	2.202	0.797
787.8	7.150	35.0430	31.0143	1.59	17.01	2171.1	2300.0	2293.3	512.7	2.027	0.808
826.1	7.612	35.1257	31.1840	1.54	15.75	2176.8	2310.0	2304.2	508.9	2.060	0.805
886.7	7.019	35.1196	31.5531	1.46	15.49	2170.5	2305.9	2300.9	484.2	2.048	0.803
930.2	7.095	35.1572	31.7733	1.51	16.15	2177.6	2311.6	2306.2	493.9	2.015	0.805
986.6	5.889	35.0026	32.0948	1.59	18.75	2168.0	2296.4	2290.9	479.9	1.919	0.810
1138.0	5.754	35.0965	32.8848	1.42	16.13	2163.8	2302.7	2298.9	440.9	1.960	0.800
1395.9	4.660	35.0257	34.1766	1.30	15.18	2146.2	2292.4	2289.6	391.9	1.913	0.794
1621.0	4.110	34.9914	35.2602	1.23	14.91	2133.8	2285.1	2282.6	365.4	1.865	0.789
1879.1	3.694	34.9682	36.4806	1.19	15.74	2124.1	2277.0	2274.3	351.4	1.770	0.787
2145.1	3.423	34.9578	37.7239	1.19	17.64	2122.9	2274.6	2271.9	347.6	1.656	0.789
2386.4	3.202	34.9507	38.8449	1.21	20.66	2123.4	2276.2	2273.4	341.0	1.578	0.789
2633.8	3.029	34.9434	39.9819	1.23	23.34	2123.3	2276.8	2273.8	336.0	1.498	0.789
2893.9	2.851	34.9358	41.1750	1.25	26.46	2123.3	2276.2	2273.1	333.3	1.408	0.790
3142.0	2.703	34.9266	42.3077	1.26	28.43	2126.1	2276.8	2272.9	336.4	1.318	0.792
3377.4	2.570	34.9176	43.3724	1.28	30.77	2124.5	2276.1	2272.9	329.6	1.257	0.792
3635.9	2.465	34.9074	44.5304	1.30	33.47	2124.6	2277.6	2274.2	324.3	1.197	0.791
3898.9	2.397	34.9000	45.7022	1.33	36.21	2126.3	2278.6	2274.9	324.4	1.127	0.792
4125.8	2.327	34.8917	46.7090	1.36	38.75	2128.1	2278.6	2275.1	325.8	1.062	0.795
4372.0	2.286	34.8824	47.7946	1.42	44.17	2128.8	2276.5	2272.8	330.2	0.992	0.798
4609.6	2.219	34.8718	48.8378	1.47	48.36	2133.4	2279.2	2275.4	333.4	0.933	0.800
4867.8	2.262	34.8751	49.9655	1.42	45.07	2128.1	2273.2	2269.6	332.8	0.880	0.801
5115.3	2.229	34.8705	51.0438	1.46	47.54	2129.1	2272.6	2268.9	335.0	0.828	0.803
5366.7	2.288	34.8729	52.1285	1.48	47.99	2121.5	2265.1	2261.5	332.9	0.785	0.803
5697.8	2.135	34.8523	53.5585	1.51	53.82	2134.2	2277.3	2273.4	333.7	0.732	0.804

Appendix 7

Table A7. South Atlantic Ocean

Depth	Temp.	Salinity	sigma_t	PO_4	SiO_4	TCO_2*	TA*	TA*(n)	pCO_2	Ω_c	Ψ
18.0	23.565	35.9590	24.5118	0.14	1.58	2101.2	2432.7	2428.3	379.6	5.438	0.622
77.9	20.483	36.1216	25.7486	0.34	2.23	2149.7	2451.3	2447.6	390.6	4.864	0.653
126.8	16.927	35.7862	26.6390	0.64	3.78	2158.3	2404.2	2389.6	443.8	4.018	0.701
183.9	14.700	35.4741	27.1873	0.83	4.99	2150.5	2363.3	2353.3	455.6	3.507	0.728
228.0	14.071	35.3787	27.4554	0.85	5.03	2142.9	2347.2	2336.9	459.1	3.359	0.735
287.8	12.375	35.1539	27.9057	1.08	6.83	2143.7	2322.2	2309.7	491.8	2.972	0.759
320.5	10.974	34.9823	28.1945	1.42	9.85	2155.8	2300.6	2288.0	565.3	2.504	0.790
390.7	10.088	34.8820	28.5980	1.49	10.80	2154.0	2293.3	2279.5	564.7	2.400	0.795
426.2	9.164	34.7720	28.8346	1.60	12.79	2149.2	2275.5	2264.6	575.3	2.206	0.808
489.1	8.528	34.6987	29.1740	1.65	13.43	2143.9	2272.2	2261.9	546.7	2.197	0.806
523.3	7.325	34.5987	29.4516	1.92	18.10	2154.2	2260.6	2252.5	594.1	1.903	0.828
590.9	6.740	34.5287	29.7928	1.89	18.21	2144.6	2256.9	2248.7	551.9	1.940	0.822
627.4	5.804	34.4656	30.0522	2.05	22.68	2151.0	2248.3	2241.4	584.1	1.741	0.837
689.5	5.740	34.4301	30.3171	1.96	20.52	2135.6	2245.1	2238.1	529.1	1.853	0.825
736.3	4.862	34.4079	30.6376	2.09	26.77	2147.3	2241.6	2235.3	567.0	1.654	0.840
790.1	4.735	34.4104	30.9036	2.13	27.28	2151.2	2252.6	2245.9	538.5	1.715	0.834
826.6	4.442	34.4057	31.1078	2.16	29.97	2148.1	2246.7	2240.7	538.2	1.663	0.837
888.3	4.277	34.3852	31.3979	2.11	29.87	2145.2	2245.2	2239.3	526.7	1.653	0.836
930.5	3.931	34.4130	31.6592	2.12	34.31	2153.5	2247.9	2242.4	541.2	1.575	0.841
989.2	3.958	34.4707	31.9717	2.17	34.56	2162.3	2260.6	2255.3	529.6	1.595	0.838
1148.4	3.796	34.5993	32.8264	2.07	36.72	2169.5	2272.6	2267.7	509.4	1.583	0.834
1611.1	3.614	34.8648	35.1815	1.60	31.23	2161.1	2296.1	2290.5	408.6	1.718	0.805
1877.5	3.317	34.8880	36.4589	1.53	33.03	2158.2	2298.5	2293.4	386.5	1.664	0.801
2144.1	3.086	34.9019	37.7176	1.47	34.38	2153.4	2294.9	2287.0	383.7	1.578	0.800
2367.4	2.936	34.9063	38.7553	1.46	35.82	2152.0	2296.9	2291.5	365.9	1.525	0.798
2614.0	2.771	34.9027	39.8921	1.46	38.36	2151.2	2296.5	2287.7	368.1	1.450	0.797
2879.6	2.608	34.8929	41.1083	1.48	42.21	2153.0	2298.5	2294.5	353.4	1.362	0.798
3090.2	2.435	34.8562	42.0255	1.61	52.60	2159.5	2297.5	2291.4	372.2	1.292	0.806
3152.9	2.452	34.8853	42.3531	1.50	45.74	2151.7	2296.7	2292.4	350.7	1.279	0.799
3374.3	2.348	34.8807	43.3556	1.50	47.54	2151.3	2297.0	2292.3	347.2	1.223	0.799
3639.8	2.135	34.8617	44.5599	1.55	54.42	2154.5	2298.8	2293.6	347.4	1.144	0.801
3892.5	1.916	34.8405	45.7037	1.62	62.09	2158.7	2298.8	2293.5	352.8	1.055	0.805
4125.4	1.530	34.8000	46.7718	1.78	77.75	2170.3	2301.1	2295.6	369.4	0.947	0.815
4358.0	1.247	34.7693	47.8295	1.89	90.08	2176.7	2300.2	2294.4	383.5	0.859	0.823
4607.8	1.090	34.7526	48.9447	1.94	95.93	2179.9	2301.1	2295.2	386.4	0.802	0.825
4882.6	1.033	34.7425	50.1557	1.98	99.58	2177.0	2295.2	2288.7	393.0	0.740	0.828
5112.3	0.922	34.7301	51.1716	2.03	104.44	2178.1	2292.2	2286.2	399.9	0.685	0.832
5373.0	0.855	34.7211	52.3146	2.04	107.07	2177.9	2289.5	2283.5	404.1	0.637	0.835
5669.5	0.802	34.7124	53.6045	2.08	110.31	2178.0	2283.9	2278	418.3	0.575	0.840

Appendix 8

Table A8. Indian Ocean.

Depth	Temp.	Salinity	sigma_t	PO_4	SiO_4	TCO_2*	TA*	TA*(n)	pCO_2	Ω_c	Ψ
18.6	25.016	35.1319	23.4259	0.26	2.73	1995.0	2320.2	2316.8	365.3	5.488	0.614
72.9	22.004	35.2992	24.6614	0.66	6.20	2067.0	2337.2	2320.0	455.7	4.538	0.669
123.4	18.558	35.3375	25.8690	1.14	12.03	2134.8	2340.4	2317.4	582.2	3.516	0.732
173.7	15.894	35.2917	26.7134	1.35	15.84	2162.5	2337.2	2313.9	628.9	3.034	0.762
223.5	14.481	35.3187	27.2859	1.41	17.18	2177.5	2341.2	2317.7	639.2	2.845	0.773
273.3	13.632	35.3333	27.7207	1.53	19.20	2193.4	2343.0	2321.6	669.9	2.624	0.786
322.3	12.000	35.1305	28.1136	1.50	19.11	2173.3	2321.5	2299.2	623.0	2.573	0.787
380.5	11.469	35.0949	28.4650	1.53	19.91	2172.4	2316.7	2297.2	612.0	2.484	0.791
418.2	10.944	35.0610	28.7059	1.66	22.30	2179.5	2314.0	2292.9	645.1	2.346	0.800
483.2	10.337	34.9869	29.0598	1.70	24.26	2175.1	2306.2	2288.3	626.2	2.260	0.803
513.6	10.041	34.9825	29.2423	1.79	26.61	2181.7	2307.9	2288.2	648.1	2.192	0.808
588.2	9.491	34.9536	29.6614	1.98	33.92	2196.0	2308.7	2293.0	680.1	1.988	0.821
616.5	9.328	34.9181	29.7939	1.93	31.98	2187.1	2304.0	2287.0	657.8	2.027	0.817
686.8	8.656	34.8987	30.2098	2.13	41.26	2205.6	2308.2	2295.4	691.4	1.823	0.831
718.8	8.409	34.8529	30.3631	2.10	40.32	2197.0	2303.7	2289.9	665.4	1.855	0.827
786.3	7.726	34.8702	30.7922	2.34	52.65	2224.4	2314.2	2304.3	718.9	1.632	0.844
817.3	7.340	34.7630	30.9177	2.24	47.97	2202.8	2300.7	2289.6	663.4	1.705	0.837
886.5	6.774	34.7842	31.3367	2.40	59.84	2225.2	2311.2	2302.6	701.2	1.546	0.849
920.9	6.224	34.7069	31.5208	2.41	60.98	2217.9	2305.9	2297.2	670.5	1.551	0.847
987.4	6.266	34.8215	31.9039	2.56	72.23	2248.1	2325.7	2318.2	731.7	1.425	0.857
1130.5	5.205	34.7307	32.6476	2.55	77.84	2241.6	2320.9	2313.4	685.2	1.387	0.856
1385.5	4.231	34.7452	33.9678	2.59	91.80	2254.6	2332.6	2326.1	660.8	1.289	0.859
1621.3	3.480	34.7542	35.1601	2.56	101.20	2259.1	2340.7	2334.3	622.1	1.246	0.857
1888.8	2.819	34.7513	36.4728	2.47	108.91	2256.5	2345.5	2338.7	571.2	1.226	0.851
2149.8	2.390	34.7493	37.7225	2.40	112.91	2252.0	2346.3	2340.1	533.9	1.192	0.847
2394.0	2.131	34.7461	38.8684	2.34	114.23	2244.7	2344.7	2338.1	504.4	1.167	0.842
2624.8	1.945	34.7445	39.9413	2.33	117.83	2244.5	2345.6	2337.5	499.8	1.117	0.842
2889.4	1.790	34.7421	41.1596	2.30	119.18	2239.7	2344.3	2337.9	475.5	1.071	0.839
3145.8	1.629	34.7361	42.3359	2.30	122.58	2239.0	2344.5	2338.0	467.6	1.016	0.839
3390.9	1.493	34.7296	43.4529	2.29	125.23	2236.6	2342.8	2335.2	463.6	0.966	0.838
3632.8	1.423	34.7262	44.5433	2.28	126.60	2232.5	2340.8	2334.7	448.5	0.925	0.837
3892.0	1.333	34.7223	45.7124	2.26	125.40	2223.6	2333.1	2327.1	438.6	0.878	0.836
4141.2	1.237	34.7176	46.8328	2.24	125.49	2218.1	2328.0	2321.9	433.2	0.831	0.836
4383.2	1.194	34.7150	47.9095	2.23	125.30	2212.8	2322.6	2316.5	429.8	0.787	0.836
4634.9	1.208	34.7134	49.0108	2.23	125.44	2211.2	2321.0	2315.0	428.1	0.746	0.837
4885.0	1.144	34.7100	50.1213	2.22	124.62	2204.7	2314.5	2308.5	423.9	0.705	0.837
5128.8	1.142	34.7097	51.1864	2.22	123.46	2200.3	2310.2	2304.3	421.0	0.669	0.837
5350.5	1.168	34.7094	52.1432	2.21	122.76	2198.0	2307.4	2301.4	421.7	0.636	0.838
5779.1	1.219	34.7110	53.9868	2.19	120.93	2190.9	2299.1	2293.2	422.3	0.577	0.839

Appendix 9

Table A9. Antarctic Ocean.

Depth	Temp.	Salinity	sigma_t	PO_4	SiO_4	TCO_2*	TA*	TA*(n)	pCO_2	Ω_c	Ψ
22.5	3.332	34.0052	27.0504	1.50	24.76	2067.7	2222.1	2214.2	341.1	2.781	0.779
76.0	2.624	34.1162	27.4638	1.66	29.89	2090.3	2234.3	2226.0	359.7	2.590	0.791
126.0	2.450	34.2424	27.8503	1.84	38.91	2120.3	2246.8	2238.1	409.8	2.315	0.809
176.9	2.729	34.3300	28.1551	1.92	44.80	2138.1	2257.0	2248.1	442.9	2.189	0.816
224.5	3.030	34.4099	28.4237	1.95	49.44	2152.7	2265.5	2257.0	471.5	2.087	0.823
278.2	2.950	34.4576	28.7273	2.01	54.19	2162.9	2273.1	2265.1	479.8	2.026	0.826
323.7	3.002	34.4724	28.9532	2.03	55.46	2166.1	2273.8	2266.2	489.0	1.972	0.828
381.2	3.220	34.4850	29.2132	2.01	54.24	2164.8	2274.8	2267.1	485.8	1.977	0.826
419.9	3.008	34.5087	29.4383	2.04	58.74	2173.6	2277.6	2270.8	500.9	1.882	0.832
484.0	2.905	34.5230	29.7669	2.07	61.43	2176.3	2281.3	2274.6	495.2	1.865	0.832
516.7	2.958	34.5166	29.9110	2.08	60.23	2176.5	2279.1	2272.6	504.1	1.823	0.834
587.2	2.668	34.5365	30.2906	2.09	64.19	2179.5	2285.0	2278.6	487.8	1.822	0.832
620.5	2.869	34.5527	30.4360	2.08	64.78	2182.8	2284.3	2278.0	506.5	1.766	0.835
687.4	2.819	34.5248	30.7406	2.10	64.37	2178.1	2281.7	2275.8	494.4	1.758	0.834
722.2	2.843	34.5642	30.9288	2.10	66.94	2185.1	2286.0	2280.1	506.8	1.716	0.836
785.8	2.583	34.5473	31.2477	2.15	69.25	2185.8	2286.5	2280.8	500.4	1.683	0.837
820.8	2.501	34.5891	31.4526	2.14	73.56	2193.3	2291.3	2285.8	510.1	1.640	0.840
885.3	2.523	34.5529	31.7249	2.16	71.16	2187.5	2287.2	2281.8	501.4	1.634	0.838
922.7	2.437	34.5995	31.9467	2.16	75.32	2195.7	2292.8	2287.4	511.3	1.591	0.841
986.6	2.100	34.6004	32.2852	2.19	80.30	2197.1	2296.5	2290.8	496.7	1.586	0.839
1129.3	2.096	34.6107	32.9604	2.19	81.66	2199.3	2296.2	2290.7	504.3	1.511	0.842
1390.2	1.666	34.6602	34.2654	2.20	92.13	2207.0	2304.6	2298.8	494.1	1.423	0.842
1622.8	1.505	34.6812	35.3812	2.20	97.09	2209.2	2306.7	2300.9	490.3	1.347	0.843
1889.4	1.345	34.7000	36.6494	2.18	101.47	2208.8	2308.0	2302.4	478.5	1.278	0.842
2148.0	1.228	34.7091	37.8636	2.17	104.80	2208.1	2308.3	2302.7	470.6	1.211	0.841
2402.4	1.012	34.7094	39.0613	2.18	109.61	2206.4	2307.4	2301.7	461.8	1.146	0.841
2631.2	0.909	34.7087	40.1225	2.17	111.74	2204.7	2305.5	2299.8	458.2	1.084	0.842
2894.0	0.781	34.7053	41.3372	2.18	115.75	2202.4	2303.6	2297.8	452.0	1.023	0.842
3133.3	0.690	34.7026	42.4359	2.18	117.14	2200.4	2301.2	2295.5	449.3	0.965	0.842
3383.8	0.576	34.6980	43.5843	2.18	119.52	2197.2	2298.2	2292.2	444.8	0.911	0.842
3624.2	0.535	34.6958	44.6735	2.18	120.91	2196.1	2297.1	2291.2	441.9	0.864	0.843
3892.0	0.375	34.6884	45.8971	2.20	124.40	2192.0	2294.1	2287.9	433.9	0.816	0.842
4127.7	0.294	34.6860	46.9660	2.19	125.22	2190.8	2290.8	2284.9	436.2	0.763	0.844
4390.3	0.340	34.6862	48.1275	2.19	126.83	2187.9	2289.3	2283.2	431.1	0.727	0.843
4629.3	0.326	34.6852	49.1892	2.20	129.56	2186.4	2286.6	2280.6	433.1	0.683	0.845
4882.2	0.307	34.6811	50.3066	2.20	130.71	2182.7	2284.4	2277.7	427.8	0.653	0.844
5117.7	0.316	34.6786	51.3377	2.21	130.55	2178.9	2282.8	2276.2	419.0	0.630	0.842
5356.1	0.307	34.6749	52.3770	2.19	128.70	2175.3	2281.5	2275.3	409.0	0.606	0.840
5776.2	0.336	34.6722	54.1881	2.24	126.35	2181.7	2290.2	2284.3	402.1	0.565	0.839